

Vapor-liquid equilibrium data for the carbon dioxide and oxygen (CO₂ + O₂) system at the temperatures 218, 233, 253, 273, 288 and 298 K and pressures up to 14 MPa

Snorre Foss Westman^{a,*}, H. G. Jacob Stang^b, Sigurd W. Løvseth^{b,**}, Anders Austegard^b, Ingrid Snustad^b, Ivar S. Ertesvåg^a

^aNorwegian University of Science and Technology, Department of Energy and Process Engineering, Kolbjørn Hejes vei 1b, NO-7491 Trondheim, Norway

^bSINTEF Energy Research, NO-7465 Trondheim, Norway

Abstract

Accurate thermophysical data for the CO₂-rich mixtures relevant for carbon capture, transport and storage (CCS) are essential for the development of the accurate equations of state (EOS) and models needed for the design and operation of the processes within CCS. Vapor-liquid equilibrium measurements for the binary system CO₂+O₂ are reported at 218, 233, 253, 273, 288 and 298 K, with estimated standard uncertainties of maximum 8 mK in temperature, maximum 3 kPa in pressure, and maximum 0.0031 in the mole fractions of the phases in the mixture critical regions, and 0.0005 in the mole fractions outside the critical regions. These measurements are compared with existing data. Although some data exists, there are little trustworthy literature data around critical conditions, and the measurements in the present work indicate a need to revise the parameters of existing models. The data in the present work has significantly less scatter than most of the literature data, and range from the vapor pressure of pure CO₂ to close to the mixture critical point pressure at all six temperatures. With the measurements in the present work, the data situation for the CO₂+O₂ system is significantly improved, forming the basis to develop better equations of state for the system. A scaling law model is fitted to the critical region data of each isotherm, and high accuracy estimates for the critical composition and pressure are found. The Peng-Robinson EOS with the alpha correction by Mathias and Copeman, the mixing rules by Wong and Sandler, and the NRTL excess Gibbs energy model is fitted to the data in the present work, with a maximum absolute average deviation of 0.01 in mole fraction.

Keywords:

vapor-liquid equilibrium, experimental measurements, carbon dioxide, oxygen, CO₂ capture and storage

1. Introduction

In the present study, vapor-liquid equilibrium (VLE) measurements for the CO₂+O₂ system are presented. It follows Westman et al. [1], which investigated the VLE of the CO₂+N₂ system. The need for new data for these systems and the other mixtures relevant for carbon capture, transport and storage (CCS) has been discussed for instance in the recently reported comprehensive literature studies by [2, 3, 4, 5]. Calculations using existing equations of state (EOS) [3, 6] show that even small amounts of impurities in CO₂-rich mixtures can significantly affect the behavior of the fluid [5, 7]. As an example, the maximum pressure at which a mixture of CO₂ and 5% O₂ can be in the two-phase region, the cricondenbar, will increase to approximately 8.4 MPa compared to the critical pressure of CO₂, 7.3773 MPa. Even with the recent progress of molecular modeling, empirical equations of state still provide the most accurate description of thermodynamic properties of such systems. Accurate data are required in order to develop such accurate models needed for the design and operation of various processes

within CCS. In the development and fitting of the highly flexible and potentially accurate multi-parameter equation of state EOS-CG for CCS mixtures, the development of the model for the CO₂+O₂ system suffered from the lack of high quality data [3, 4]. For instance, some of the seemingly most accurate available vapor-liquid equilibrium data for the CO₂+O₂ system were not consistent with the vapor pressure of pure CO₂ [3, 4], indicating an error in the measured pressure, temperature or composition of these data. The objective of the measurements in the present work was to reconcile the inconsistencies and cover gaps in the available literature data, including states close to critical conditions and temperatures above 273.15 K, where little data of sufficient quality existed.

The work presented here was part of a project called CO₂Mix. As described by Løvseth et al. [7, 8], the CO₂Mix project aimed at performing accurate vapor-liquid equilibrium, speed of sound and density measurements of CO₂-rich mixtures at conditions relevant for transport and conditioning in CCS [5, 9]. As part of this project, a setup has been specifically designed and constructed in order to perform highly accurate phase equilibria measurements on CO₂-rich mixtures under relevant conditions for CCS. This setup has been described in detail in [10, 1]. The experimental appara-

*Corresponding author.

**Corresponding author.

Email addresses: snorre.f.westman@ntnu.no (Snorre Foss Westman), sigurd.w.lovseth@sintef.no (Sigurd W. Løvseth)

tus was validated by the VLE measurements on the CO₂+N₂ system performed by Westman et al. [1], as data of high quality were available for this system.

In the present paper, VLE measurements for the CO₂+O₂ system are reported for six isotherms at 218.15, 233.14, 253.15, 273.15, 288.14 and 298.14 K, spanning the region from close to the triple point temperature to close to the critical temperature of pure CO₂. The pressure ranges from 0.56 to 14.4 MPa. Comparison with existing data and EOSs are provided. Furthermore, an EOS is fitted to the data, with the possibility for use over the whole temperature range of the experimental data.

Special care has been taken to present the results and analysis in accordance with the IUPAC Guidelines for reporting of phase equilibrium measurements given in the work by Chirico et al. [11]. In particular, a thorough estimation of the standard uncertainties, as specified in the ISO Guide for the Estimation of Uncertainty in Measurement, commonly referred to as “GUM” [12], has been performed.

In the following the experimental setup and procedures are described in Section 2, the uncertainty analysis in Section 3. Results will be presented, discussed and analyzed in Sections 4 and 5, including fitting of EOS parameters before conclusions are drawn in Section 6. The detailed experimental data for liquid, vapor and supercritical states are tabulated in Appendix A.

2. Experimental apparatus

2.1. Description of setup

The apparatus used for the VLE measurements in the present work was described in [1]. Therefore, only a short summary of the experimental setup will be given here. A diagram of the cell and apparatus is shown in Fig. 1.

As described in [1], the measurements were performed using an isothermal analytical method with a variable-volume cell. This type of methodology has been described in, for example, [13].

According to Gibbs’ phase rule, for a system of two components with two coexisting phases, only two intensive variables can be varied freely. In the experiments in the present work, the temperature and pressure were the independent variables. The equilibrium cell, kept at constant temperature using a thermostatic bath, was filled with both CO₂ and O₂ until both liquid and vapor phases were present. A stirrer was used to mix the content to a stabilization of the temperature and pressure at their equilibrium values. The liquid and vapor phase CO₂ mole fractions at VLE were then the dependent variables. The temperature and pressure were measured. After stopping the stirrer, and waiting for the phases to settle according to density, samples of both the liquid and vapor phases were withdrawn from the cell to determine the VLE phase compositions. The samples were withdrawn using RolsiTM electromagnetic samplers (Armines patent [14]. Pneumatic version of the RolsiTM sampler described in [15]), one with the capillary inlet placed in the top of the vapor

phase, and one placed in the liquid phase. Several samples were taken of both phases. The samples were analyzed using a gas chromatograph (GC) with helium as the carrier gas, calibrated against gravimetrically prepared calibration gas mixtures. To prevent a decrease in the cell pressure due to the removal of mass from the cell, a plate bellows placed inside the cell was expanded to decrease the cell volume when samples were withdrawn. The bellows could be expanded approximately 1 cm³. The equilibrium cell consisted of a transparent sapphire cylinder placed between two titanium flanges, the internal cell volume being approximately 100 cm³.

2.2. Calibration

The calibration of the temperature and pressure sensors performed in [1] was used in the present work. The calibration was performed in-house. The temperature sensors were calibrated against fixed point cells according to the International Temperature Scale of 1990 (ITS-90). The pressure sensors were calibrated against a recently calibrated dead weight tester. Details concerning the estimated temperature and pressure measurement uncertainties are given in Section 3.2 below, and discussed in detail in [1].

The GC was calibrated against calibration gas mixtures prepared in-house using our custom built apparatus for gravimetric preparation of mixtures. Details about the calibration gas mixtures and the calibration can be found in Section 3.3 below. The manufacturer’s specification of the purities of these samples are given in Table 1. No additional analysis of the specified purities was performed.

2.3. Experimental procedures

2.3.1. General

The experimental procedures were quite similar to those of [1]. The complete procedure will be given here:

Before starting a VLE experiment, the whole circuit in connection with the VLE cell was evacuated, using the vacuum pump. The evacuation included the gas lines to the cell from the gas cylinders of pure CO₂ and O₂, and all lines transporting the gases into the cell.

The CO₂ pump and O₂ impurity pump and lines were first evacuated once, and then flushed with the respective gases to dilute any remaining impurities in the lines and pumps. This evacuation and flushing were repeated 5 times for each pump. After the final evacuation, the gases were filled onto their respective lines and pumps, and maintained at a pressure of at least 0.5 MPa to prevent contamination of the gases. After the flushing of the gas lines and pumps, the cell was flushed with CO₂, and evacuated. As with the pumps, the flushing and evacuation were repeated 5 times.

Following the flushing, and with the thermostatic bath kept at the desired temperature, CO₂ was injected until the volume fraction of liquid CO₂ was approximately 25% of the cell. The stirrer then ran until the measured pressure and temperature had stabilized. After the stirrer had been turned

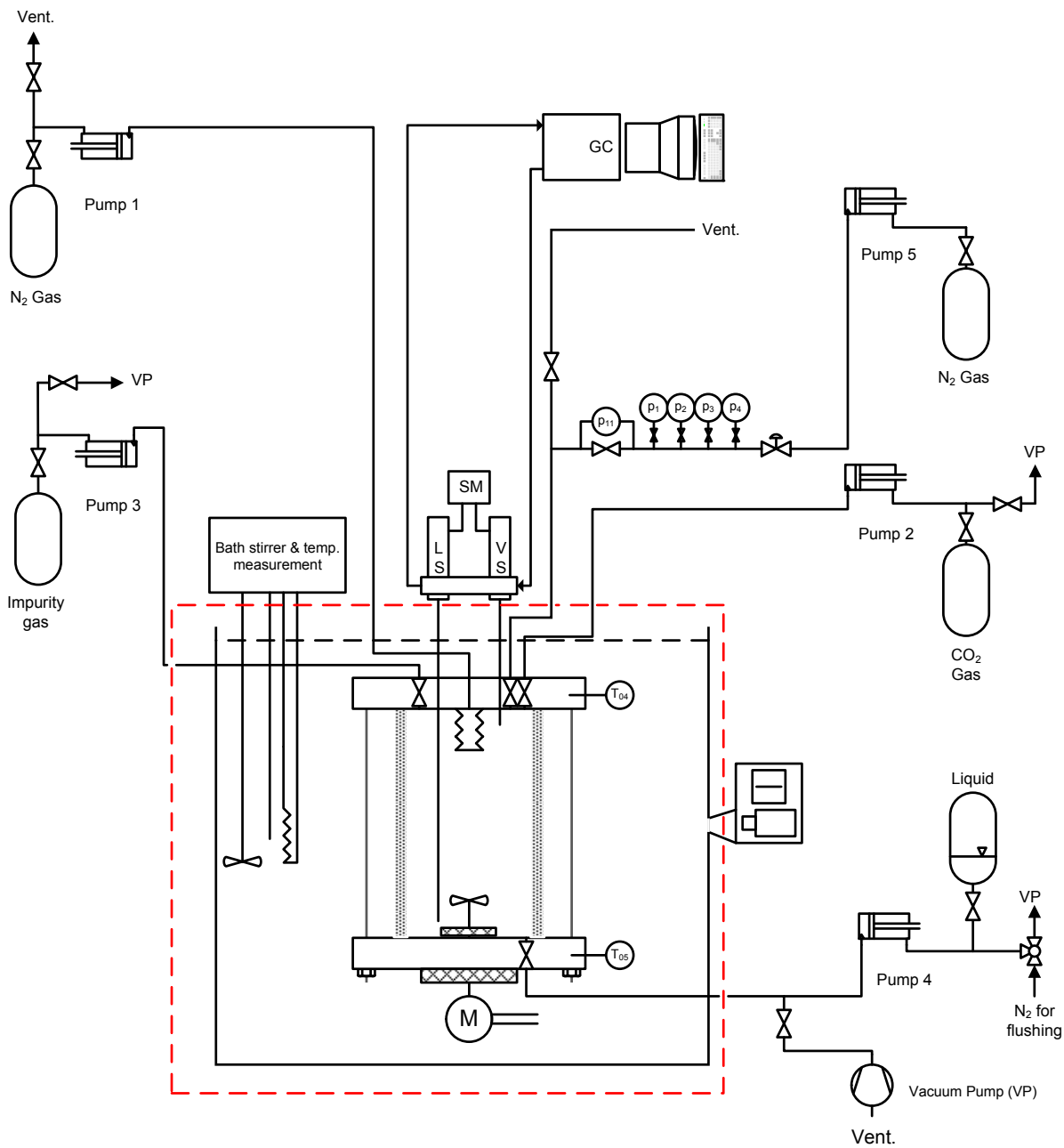


Fig. 1. Figure modified from [1]: Principal diagram of cell and ancillary apparatus. LS,VS: Liquid and vapor phase Rolsi™ samplers, respectively. SM: Rolsi™ controller. M: Gear for rotating permanent magnet below cell, which rotates stirrer inside cell. Gear connected to electric motor outside bath. T₀₄: Top flange SPRT. T₀₅: Bottom flange SPRT.

off, the vapor pressure of CO₂ was measured. If the measured vapor pressure were within the combined uncertainty of the Span-Wagner EOS [6] and our measurements, the purity of the CO₂ in the cell, and the accuracy of the current temperature and pressure measurements, were deemed to be sufficient.

After the CO₂ vapor pressure measurements, the stirrer was started and O₂ was filled onto the cell to increase the pressure. As part of the process of adjusting the pressure to the desired level, the volume fraction of liquid phase in the cell was adjusted to allow for as large as possible vapor samples, either by injecting more CO₂ or venting out some of the vapor or liquid phase. Based on VLE calculations using EOS-CG [3] for the CO₂+O₂ mixture, at constant temperature, as the pressure increased from the vapor pressure of CO₂ up to the critical pressure of the mixture, the difference between the densities of the liquid and vapor phases decreased: the density of the liquid phase decreased and that of the vapor phase increased, and ultimately approached the same value at the critical point. Taking this behavior into account, and considering the limitations of the stirrer size on the minimum liquid level, the liquid volume fraction was adjusted to around 25% for the VLE measurements at the lowest pressures at each temperature, and was gradually increased to around 50% for the measurements in the critical region.

When the pressure and temperature measurements had been stable for at least 20 min, the stirrer was turned off, and the vapor and liquid phases were left to settle before sampling started. The time allowed for settlement of the phases ranged from 30 min to 3 hours, depending on the proximity to the mixture critical pressure. At pressures between the CO₂ vapor pressure and the turning point in the vapor phase composition, the difference in densities of the liquid and vapor phase was quite large, and for these measurements we waited around 30 min for the phases to settle before sampling started. At pressures above the turning point in vapor phase composition, the settling time was increased to 1 hour.

When the pressure was increased to the point where it was observed that running the stirrer caused the phase boundary to disappear, the settling time was increased to 3 hours. At these pressures approaching the critical point, the small density difference of the phases necessitated these longer settling times. During the settling time, the borescope was used to take a picture of the cell content every 30 min. Immediately after the stirrer was turned off, both phases were cloudy white. After 2 hours, the phases were less cloudy, and it was not possible to see a difference in the opacity during

the last of these three hours.

During the settling period, the borescope was withdrawn from the thermostatic bath immediately after use to prevent unintended heat transfer from the surroundings into the bath fluid. At the end of the settling period, the borescope was put in for a very short time to confirm the existence of a liquid and vapor phase, and a visual measurement of the volume occupied by the phases was performed.

After the settling period, first the liquid and then the vapor phase was sampled. Nominally, 7 samples were taken from each phase. Upon sampling, the bellows was expanded to compensate for the pressure drop. A sample was withdrawn from the cell every 25 min. For some of the series of liquid and vapor samples at a certain temperature and pressure, we were not able to take as much as 7 samples, as we reached the maximum expansion limit of the bellows.

The same methodology as in [1] was applied to determine the sample size necessary to flush the Rolsi™ capillaries. The first sample from each phase was discarded as a flushing sample.

The pressure sensor readings were logged every second, and ratios of the temperature sensors were logged approximately every 20 seconds. The temperature and pressure measurements in the stable period before the first sample and until the last sample formed the data set for a VLE point measurement series. The treatment of these data sets is described in Section 3.4.

2.3.2. Critical region

At the temperatures 218.15, 233.14, 253.15 and 273.15 K, a special procedure was employed to perform measurements close to the critical point of the mixture at each temperature. In each of these measurement series at constant temperature and pressure, the removal of mass from the cell through the sampling lowered the equilibrium pressure for the following measurement series. This allowed for very small pressure steps compared to the general procedure described earlier, where CO₂ or O₂ was filled onto or removed from the cell using the pumps or the venting valve.

The procedure was as follows: The cell pressure was first increased to as close to the critical pressure as possible, while keeping the liquid volume fraction close to 50%. As mentioned earlier, the close proximity to the critical point was established by observing at which pressure the phases became indistinguishable when the stirrer was running. In addition, at this point the injection of very small amounts of either CO₂ or O₂ caused very large changes to the liquid phase volume

Table 1
Chemical samples used.

| Chemical name | CASRN | Source | Initial mole fraction purity | Purification method | Final mole fraction purity | Analysis method |
|-----------------------------|-----------|------------------|------------------------------|---------------------|----------------------------|-----------------|
| Carbon dioxide ^a | 124-38-9 | Yara Praxair/AGA | 0.99999 | None | 0.99999 | None |
| Oxygen ^b | 7782-44-7 | Yara Praxair | 0.999999 | None | 0.999999 | None |
| Helium ^c | 7440-59-7 | AGA | 0.999999 | None | 0.999999 | None |

^a Maximum specified impurity content by volume was less than 2 ppm H₂O, 1 ppm O₂, 5 ppm N₂, 1 ppm hydrocarbons C_nH_m and 1 ppm H₂.

^b Maximum specified impurity content by volume was less than 0.5 ppm H₂O, 1 ppm N₂, 0.5 ppm Ar, 0.02 ppm methane CH₄, 0.1 ppm CO₂ and 0.2 ppm CO. Manufacturer's specification states that total impurity level was not above 1 ppm. ^c GC carrier gas.

fraction, as could be expected when the cell content was very close to the mixture critical point, but still in the two-phase region.

With the cell content in this state, at a pressure slightly below the critical pressure and with a liquid volume fraction of approximately 50%, the bellows was expanded slightly to increase the cell pressure. If the cell content was sufficiently close to the critical pressure before this pressure increase, the cell content would move out of the two-phase region into the supercritical region. With the stirrer running, this transition out of the two-phase region seemed to be discernible by the disappearance of a swirling motion of the cell content. At this state, it was not possible to observe any qualitative difference in the appearance of the cell content when the stirrer was running, compared to when it was stopped.

The bellows was then used to keep the cell pressure stable, and the stirrer was run for between 30 min and 2 hours, and then stopped. Given the possibility that the cell content could still be in the two-phase region, without any liquid-vapor phase boundary visible using the borescope, the cell content was allowed to settle for 2-3 hours.

Then, samples were withdrawn from the liquid and vapor phase, following the sampling procedure described earlier. After the sampling was finished, the stirrer was started, and the bellows was compressed by lowering the pressure on the bellows circuit. For the critical region measurements for the four temperatures mentioned earlier, the decrease in pressure brought the cell content back into the two-phase region, visible by the swirling motion of the cell content, and the separation of the content into a liquid and vapor phase when the stirrer was stopped.

With the bellows keeping the cell pressure constant at this new lowered pressure, the process of stirring and settling was repeated, and samples were withdrawn from both phases.

This procedure of starting at a pressure slightly into the supercritical region, and using the bellows to keep the pressure stable while samples were taken, and then repeating this at a lowered pressure using the bellows, allowed us to perform several VLE measurements very close to the critical point of the mixture. For each of the temperatures 218.15, 233.14, 253.15 and 273.15 K, this resulted in 2-3 VLE measurements very close to the critical point, and 1 pressure-temperature-composition state point in the supercritical region. Details concerning these measurements are presented in Sections 4 and 5.

3. Uncertainty analysis

3.1. Definitions

The terms and definitions in the “GUM” [12] is used in the uncertainty analysis. The uncertainties are evaluated as standard uncertainties, with symbol $u(y)$, where y is the estimate of the measurand Y . The propagation of the standard uncertainties in input quantities X_i into a final calculated value Y is described by the combined standard uncertainty, with symbol $u_c(y)$.

3.2. Pressure and temperature

A thorough analysis of the uncertainty of the pressure and temperature measurements was performed in [1], where VLE measurements of the CO_2+N_2 system were performed. The same methodology was used for the measurements in the present work, the only difference being that the density used in the hydrostatic pressure calculations was calculated using EOS-CG for CO_2+O_2 instead of CO_2+N_2 . Only the resulting uncertainty estimates are given here. The details of the uncertainty analysis methodology can be found in [1].

The uncertainty components contributing to the standard uncertainty for the measured pressure p at VLE are summarized in Table 2, and the resulting standard uncertainties in the pressure measurements are shown in Fig. 2. Similarly, Table 3 and Fig. 3 show the contributors to and the resulting standard uncertainty in the measured temperatures T .

As seen from Fig. 2, the standard uncertainty in the pressure was estimated to be below 0.05% of the measured pressure except at the lowest pressure. Similarly, as seen from Tables 7 and 8 and Fig. 3, the standard uncertainty in the temperature was estimated to be below 8 mK, and the variation in temperature had been less than 5 mK.

Table 2

Summary of standard uncertainty components for pressure measurements, cf. Westman et al. [1].

| Symbol | Description and unit | u |
|--------------------------------|--|---|
| Hydrostatic pressure p_{hs} | | |
| $u(\rho_1)$ | EOS-CG ^a vapor density of CO ₂ +O ₂ (kg m ⁻³) | $1 \cdot 10^{-2} \cdot \rho_1$ |
| $u(\rho_2)$ | Same as $u(\rho_1)$ (kg m ⁻³) | $1 \cdot 10^{-2} \cdot \rho_2$ |
| $u(\rho_{4,1})$ | SW ^b density at 313.15 K (kg m ⁻³) | $3 \cdot 10^{-4} \cdot \rho_{4,1}$ |
| $u(\rho_{4,2})$ | Same as $u(\rho_1)$ (kg m ⁻³) | $1 \cdot 10^{-2} \cdot \rho_{4,2}$ |
| $u(\text{CAD})$ | (m) | 0 |
| $u_c(h_1)$ | (m) | 0.0048 |
| $u(h_{liq})$ | (m) | 0.0048 |
| $u(h_{liq,1})$ | Borescope h_{liq} (m) | 0.0048 |
| $u(h_{liq,2})$ | Variation in h_{liq} (m) | 0 |
| $u(h_2)$ | Bath liquid level variation (m) | 0.006 |
| $u_c(h_3)$ | (m) | 0.006 |
| $u(h_4)$ | Same as $u(\text{CAD})$ (m) | 0 |
| $u(g_1)$ | Local g (m s ⁻²) | $2 \cdot 10^{-7}$ |
| Differential pressure p_{11} | | |
| $u(p_{11,1})$ | Ambient temperature (MPa) | 0 |
| $u(p_{11,2})$ | Line pressure zero (MPa) | 0 |
| $u(p_{11,3})$ | Line pressure span (MPa) | $4.9 \cdot 10^{-5} \text{ MPa}^{-1} \cdot p_i \cdot p_{11}$ |
| $u(p_{11,4})$ | Mounting (MPa) | 0 |
| $u(p_{11,5})$ | Vibration (MPa) | $2.8 \cdot 10^{-5}$ |
| $u(p_{11,6})$ | Power supply (MPa) | 0 |
| $u(p_{11,7})$ | A/D conversion (MPa) | $2.4 \cdot 10^{-4}$ |
| Pressure sensors p_i | | |
| $u(p_1)$ | 1 MPa sensor (MPa) | $2.24 \cdot 10^{-4}$ |
| $u(p_2)$ | 3 MPa sensor (MPa) | $2.33 \cdot 10^{-4}$ |
| $u(p_3)$ | 10 MPa sensor (MPa) | $7.64 \cdot 10^{-4}$ |
| $u(p_4)$ | 20 MPa sensor (MPa) | $1.965 \cdot 10^{-3}$ |

^a Gernert and Span [3] and Gernert [4] ^b Span and Wagner [6]

Table 3

Summary of standard uncertainty components for temperature measurements, cf. Westman et al. [1].

| Symbol | Unit | u |
|-----------------------|--------------|----------------------|
| $u(W_b)$ | (-) | $0.35 \cdot 10^{-6}$ |
| $u(R_{ref})$ | (Ω) | $8.5 \cdot 10^{-6}$ |
| $u(T_{H_2O})$ | (mK) | 0.51 |
| $u(T_{Hg})$ | (mK) | 1.43 |
| $u(T_{Ga})$ | (mK) | 0.85 |
| $u(R_{H_2O}(T_{04}))$ | (Ω) | $3.94 \cdot 10^{-5}$ |
| $u(R_{H_2O}(T_{05}))$ | (Ω) | $2.57 \cdot 10^{-5}$ |
| $u(R_{Hg}(T_{04}))$ | (Ω) | $2.29 \cdot 10^{-5}$ |
| $u(R_{Hg}(T_{05}))$ | (Ω) | $1.84 \cdot 10^{-5}$ |
| $u(R_{Ga}(T_{04}))$ | (Ω) | $2.69 \cdot 10^{-5}$ |
| $u(R_{Ga}(T_{05}))$ | (Ω) | $2.37 \cdot 10^{-5}$ |
| $u(W_{Hg}(T_{04}))$ | (-) | $6.2 \cdot 10^{-6}$ |
| $u(W_{Hg}(T_{05}))$ | (-) | $6.1 \cdot 10^{-6}$ |
| $u(W_{Ga}(T_{04}))$ | (-) | $4.5 \cdot 10^{-6}$ |
| $u(W_{Ga}(T_{05}))$ | (-) | $4.3 \cdot 10^{-6}$ |

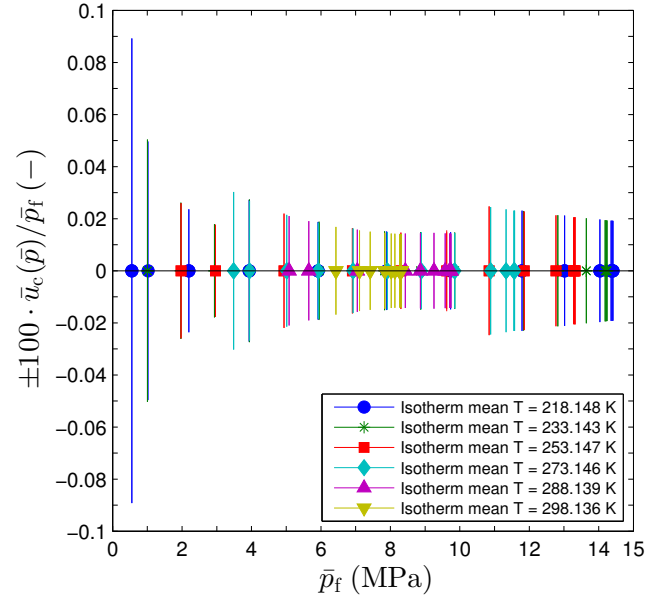


Fig. 2. Pressure standard uncertainty relative to the measured pressure for the VLE measurements performed, expressed as $100 \cdot \bar{u}_c(\bar{p})/\bar{p}_f$. Measured pressure \bar{p}_f . Standard uncertainty $\bar{u}_c(\bar{p})$.

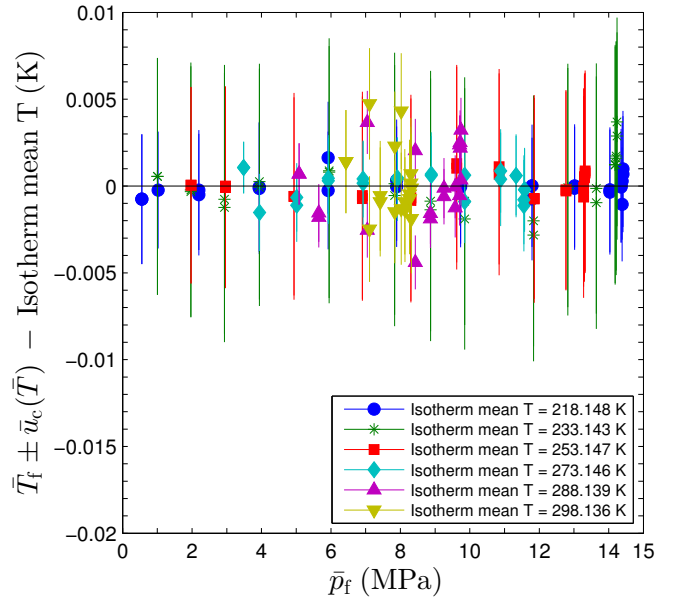


Fig. 3. Temperature deviations for each VLE measurement from isotherm mean temperature, and temperature standard uncertainty, expressed together as $\bar{T}_f \pm \bar{u}_c(\bar{T}) - \text{isotherm mean temperature}$, versus VLE experiment pressure \bar{p}_f . VLE experiment mean temperature \bar{T}_f . Temperature standard uncertainty $\bar{u}_c(\bar{T})$.

Table 4

Molar masses of atomic elements and compounds with uncertainties [17, 18].

| Component i | M_i | $u(M_i)$ | Unit |
|----------------------|------------|------------|----------------------|
| C ^a | 0.0120108 | 0.0000003 | kg mol ⁻¹ |
| O ^a | 0.01599938 | 0.0000007 | kg mol ⁻¹ |
| O ^b | 0.01599940 | 0.00000035 | kg mol ⁻¹ |
| CO ₂ | 0.0440096 | 0.0000003 | kg mol ⁻¹ |
| O ₂ | 0.03199880 | 0.00000070 | kg mol ⁻¹ |
| CO ₂ +imp | 0.0440094 | | kg mol ⁻¹ |
| O ₂ +imp | 0.03199880 | | kg mol ⁻¹ |
| CO ₂ ,eff | 0.0440097 | | kg mol ⁻¹ |
| O ₂ ,eff | 0.03199881 | | kg mol ⁻¹ |

^a In CO₂ molecule ^b In O₂ molecule

3.3. Composition

The VLE phase composition analysis and uncertainty estimation were performed in the same manner as in [1], with the methodology applied to CO₂+O₂ samples instead of CO₂+N₂. A summary will be provided here, with reference to [1] for further details.

The composition analysis was performed using the same GC as in [1], with its calibration performed using gravimetrically prepared gas mixtures using a custom-built rig in our laboratories [16].

For the measurement method utilized in the present work, it could be stated that the composition uncertainty stemmed from a range of sources, including the impurities of the gases used to prepare the calibration mixtures, the uncertainty in the molar masses, inaccuracies in the weighed masses, adsorption, repeatability / uncertainties of the sampling and GC analysis, and finally the consistency between the GC calibration function and data. The analysis of these contributing factors are given below.

3.3.1. Source gas composition and molar mass

The composition and the corresponding uncertainty of a gravimetrically prepared gas mixture are results of both the purity and the molar mass of the source gases used for the mixture. According to [17, 18], the molar masses of monoatomic carbon C, monoatomic oxygen O in commercial tank gas CO₂ and monoatomic oxygen O in commercial tank gas O₂ generally lie within ranges of width 0.6, 0.15, and 0.7 mg mol⁻¹, respectively. Based on this, the molar masses of CO₂ and O₂, M_{CO_2} and M_{O_2} respectively, were calculated with the corresponding uncertainty estimates shown in Table 4.

The minimum certified purities of the CO₂ and O₂ source gases used to prepare the calibration gas mixtures are given in Table 1, together with the manufacturers' specifications of the maximum content of certain impurities. Since the source gases were not entirely pure, estimates for the molar masses of the source gases, M_{CO_2+imp} and M_{O_2+imp} , should account for the impurities present, following the procedure used in [1].

M_{CO_2+imp} and M_{O_2+imp} were calculated based on the impurity specifications stated in Table 1. The molar mass of each impurity was calculated using data from Wieser et al.

[18], assuming methane CH₄ for the hydrocarbon impurity fraction. The molar masses of the source gases, M_{CO_2+imp} and M_{O_2+imp} , together with the effective molar masses of the source gases excluding the impurities, $M_{CO_2,eff}$ and $M_{O_2,eff}$, are shown in Table 4.

3.3.2. Gravimetric preparation

The methodology of gravimetric preparation of the calibration gas mixtures and the uncertainty estimation given in [1, 16] was used in the present work. Details are given in Appendix A.3.3 in [1].

Six CO₂+O₂ calibration gas mixtures were made, spanning in CO₂ mole fractions $y_{CO_2,cal}$ from 0.13 to 0.95. An overview of the mixtures is given in Table 5.

3.3.3. Composition calibration procedure and estimated composition uncertainty

The calibration of the GC was performed as described in Appendix A.3.1 in [1], with the measures described to prevent adsorption of the gas onto the contact surfaces. Samples of varying sizes were withdrawn from the cell at different pressures between 5 and 10 MPa. These samples formed the calibration basis for the composition analysis, establishing a relation between the CO₂ mole fractions of the calibration gas mixtures and the GC detector response.

The uncertainty contribution from the calibration mixture uncertainty reaching the GC could be estimated as

$$u_c(y_{CO_2,cal}) = \sqrt{u^2(y_{CO_2,cal}, m) + u^2(y_{CO_2,cal}, M_{eff}) + u^2(y_{CO_2,cal}, ads.)}, \quad (1)$$

where $u(y_{CO_2,cal}, m)$ and $u(y_{CO_2,cal}, M_{eff})$ are the contributing uncertainties stemming from the uncertainties in the masses of CO₂ and O₂ in the gas mixture and the uncertainties in the effective molar masses, respectively. These terms are described in detail in Appendix A.3 of [1]. The last term in Eq. (1), $u(y_{CO_2,cal}, ads.)$, is the contributing uncertainty from adsorption, and was estimated assuming that CO₂ is adsorbed at a higher degree than O₂, in the same way as in [1]. The uncertainty estimates used in Eq. (1) are given in Table 5.

As seen in Table 5, the uncertainty contribution from the molar mass of O₂ caused $u(y_{CO_2,cal}, M_{eff})$ to dominate

Table 5

CO₂+O₂ calibration gas mixtures: CO₂ mole fractions and corresponding standard uncertainties.

| $y_{CO_2,cal}$ | $u(y_{CO_2,cal}, m)$ | $u(y_{CO_2,cal}, M_{eff})$ | $u(y_{CO_2,cal}, ads.)$ | $u_c(y_{CO_2,cal})$ |
|----------------|----------------------|----------------------------|-------------------------|----------------------|
| 0.131144 | $2.7 \cdot 10^{-6}$ | $17.4 \cdot 10^{-6}$ | $1.4 \cdot 10^{-6}$ | $17.6 \cdot 10^{-6}$ |
| 0.303027 | $2.1 \cdot 10^{-6}$ | $11.2 \cdot 10^{-6}$ | $3.3 \cdot 10^{-6}$ | $11.9 \cdot 10^{-6}$ |
| 0.549780 | $2.6 \cdot 10^{-6}$ | $5.4 \cdot 10^{-6}$ | $5.9 \cdot 10^{-6}$ | $8.4 \cdot 10^{-6}$ |
| 0.686269 | $1.4 \cdot 10^{-6}$ | $4.9 \cdot 10^{-6}$ | $7.3 \cdot 10^{-6}$ | $8.9 \cdot 10^{-6}$ |
| 0.898418 | $5.1 \cdot 10^{-6}$ | $7.4 \cdot 10^{-6}$ | $9.7 \cdot 10^{-6}$ | $13.2 \cdot 10^{-6}$ |
| 0.945826 | $2.4 \cdot 10^{-6}$ | $8.2 \cdot 10^{-6}$ | $10.1 \cdot 10^{-6}$ | $13.3 \cdot 10^{-6}$ |

the combined standard uncertainty of the CO₂ mole fraction $u_c(y_{\text{CO}_2,\text{cal}})$ for the gas mixtures with the highest O₂-content. For the mixtures with the highest CO₂-content, the uncertainty contribution from the adsorption of CO₂ was the dominating factor. The uncertainty contribution from the adsorption was for all the mixtures of the same order as the two other contributing factors, and as in [1], the uncertainty of the CO₂ mole fractions of the calibration gases, $u_c(y_{\text{CO}_2,\text{cal}})$, would have to be orders of magnitude larger to be of significance for the final uncertainty in the VLE composition data. As the discussion in the following section will show, the reason for this was that the main contributor to this final uncertainty was the calibration function error.

3.3.4. GC integration and calibration function

The GC column, method and detector used for CO₂+N₂ samples in [1] were utilized on CO₂+O₂ samples in the present work, with helium as the GC carrier gas. This setup gave just as good separation of the CO₂ and O₂ peaks in the GC chromatogram as in [1] for CO₂ and N₂. The areas under the CO₂ and O₂ peaks in the chromatogram, denoted A_{CO_2} and A_{O_2} , were obtained for each sample by numerical integration. The GC thermal conductivity detector (TCD) response was nonlinear with respect to the number of moles of CO₂ and O₂ passing through the detector. The following model, consisting of both linear and nonlinear terms, described adequately the relation between moles of each component in the sample to the area of each component:

$$\hat{n}_{\text{CO}_2} \cdot k = A_{\text{CO}_2} + (A_{\text{CO}_2})^{c_1} + (A_{\text{CO}_2})^{c_2}, \quad (2)$$

$$\hat{n}_{\text{O}_2} \cdot k = c_3 \cdot (A_{\text{O}_2} + (A_{\text{O}_2})^{c_4} + (A_{\text{O}_2})^{c_5}), \quad (3)$$

$$\hat{y}_{\text{CO}_2,\text{cal}} = \frac{\hat{n}_{\text{CO}_2}}{\hat{n}_{\text{CO}_2} + \hat{n}_{\text{O}_2}}, \quad (4)$$

where $\hat{y}_{\text{CO}_2,\text{cal}}$ is the estimator of the CO₂ mole fraction of a calibration gas mixture sample given the areas for that sample, and k is an unknown factor relating the areas to the number of moles.

The parameters c_i for $i = 1$ through 5 were fitted by performing a weighted least squares minimization of the objective function S described by Eq. (A.32) in [1]. The mean values of the estimator, $\hat{y}_{\text{CO}_2,\text{cal}}$, calculated for each of the $n = 62$ series, with each series consisting of 6-9 valid samples, were fitted against the calibration mixture mole fractions, $y_{\text{CO}_2,\text{cal}}$, which resulted in the parameter estimates found in Table 6. As shown in Fig. 4, the errors between the calibration gas CO₂ mole fractions and the model predictions, $e = y_{\text{CO}_2,\text{cal}} - \hat{y}_{\text{CO}_2,\text{cal}}$, were randomly scattered around zero over the composition range $y_{\text{CO}_2,\text{cal}}$, which indicated an appropriate model structure. The sample standard deviation of the errors, $s(e)$, is also given in Table 6. This model was used to convert the areas resulting from the analysis of a composition sample taken during a VLE experiment into a CO₂ mole fraction.

For the same reasons as described in [1], it was assumed that the standard uncertainty of the CO₂ mole fraction of

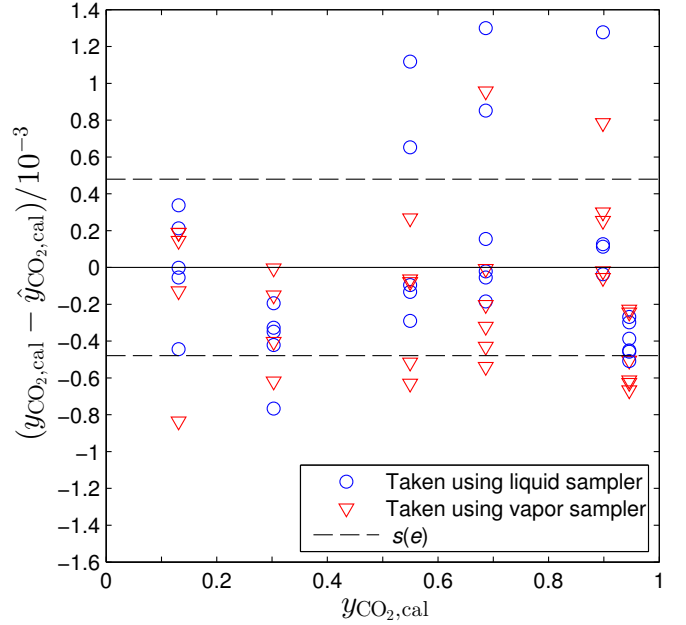


Fig. 4. Composition calibration: Error between actual compositions in Table 5 and composition model in Eq. (4), given as $y_{\text{CO}_2,\text{cal}} - \hat{y}_{\text{CO}_2,\text{cal}}$ versus $y_{\text{CO}_2,\text{cal}}$. Composition analysis uncertainty $u(x_{\text{CO}_2}) = u(y_{\text{CO}_2}) = s(e)$ from Table 6.

Table 6

Fitted parameters of the $\hat{y}_{\text{CO}_2,\text{cal}}$ model and standard uncertainty of composition analysis $u(x_{\text{CO}_2}) = u(y_{\text{CO}_2})$.

| Variable | Value |
|--|------------------------|
| c_1 | 0.899902 |
| c_2 | 1.154287 |
| c_3 | 1.270181 |
| c_4 | 1.155333 |
| c_5 | 0.914593 |
| $u(x_{\text{CO}_2}) = u(y_{\text{CO}_2}) = s(e)$ | $4.7894 \cdot 10^{-4}$ |
| n | 62 |

samples taken during VLE measurements, $u(x_{\text{CO}_2}) = u(y_{\text{CO}_2})$, was estimated by $s(e)$, which was 25-60 times larger than the standard uncertainties in the mole fractions of the calibration mixtures, $y_{\text{CO}_2,\text{cal}}$. It must be emphasized that this estimate only accounts for the uncertainty caused by the composition analysis of the samples. All other reasons that could cause the sample to not represent the actual VLE composition are not accounted for in this estimate, and these contributors could only be minimized by the measures described in Section 2.3 and in [1].

3.3.5. Total uncertainty in liquid and vapor phase mole fractions x_{CO_2} and y_{CO_2}

For a given VLE measurement, the uncertainty of T and p contributed to additional uncertainty in the composition, giving the following total standard uncertainty of the com-

position:

$$u_{\text{tot}}(z_{\text{CO}_2}) = \sqrt{u^2(z_{\text{CO}_2}) + \left(u_c(\bar{T}) \cdot \frac{\partial z_{\text{CO}_2}}{\partial T}\right)^2 + \left(u_c(\bar{p}) \cdot \frac{\partial z_{\text{CO}_2}}{\partial p}\right)^2} \quad (5)$$

where z_{CO_2} was equal to either x_{CO_2} or y_{CO_2} , and the temperature and pressure uncertainties $u_c(\bar{T})$ and $u_c(\bar{p})$ are described in [1]. The derivatives in Eq. (5) were, in general, calculated numerically from the PR-MC-WS-NRTL Case 2 EOS fitted to our data. Details about this EOS are explained in Section 5.4.2. For the VLE measurements in the critical region used to fit the scaling law in Section 5.3, the derivatives with respect to pressure, $\partial z_{\text{CO}_2}/\partial p$, were calculated analytically from the fitted scaling law in Eq. (6), as this gave better estimates for the derivatives than the PR-MC-WS-NRTL Case 2 EOS in this region. Details concerning the scaling law are given in Section 5.3.

3.4. Data reduction

The same procedure for data reduction as used in [1] was utilized in the present work, and only a short summary of the observations particular to this work and the symbols used is given here.

As described in Section 2.3, the drop in cell pressure after each composition sample was compensated using the bellows to decrease the cell volume. For the VLE measurements in this work, the cell pressure was in most cases back at its original value after around 1-3 min, and for a few of the measurements after around 5 min. After the cell pressure was back to its stable value, it remained stable for the remaining 20-24 min until the next sample was withdrawn.

In each series of either consecutive liquid or vapor phase composition samples, x_{CO_2} or y_{CO_2} , at a nominal temperature and pressure, it was assumed that each composition sample represented the equilibrium composition at the temperature \bar{T} and pressure \bar{p} before the sample was withdrawn from the cell. As in [1], the bellows was able to stabilize the cell pressure sufficiently fast after each sample withdrawal, and it was not possible to see any systematic trends in the temperature or pressure during these time periods. It was also not possible to see any temperature variations caused by the removal of mass from the cell in the composition sampling.

For each of these series of samples, the arithmetic mean values of the temperature, pressure, liquid and vapor phase compositions were calculated, denoted as \bar{T}_f , \bar{p}_f , \bar{x}_{CO_2} and \bar{y}_{CO_2} , respectively. The subscript f is used to differentiate between the temperature and pressure values associated with each composition sample x_{CO_2} or y_{CO_2} , and of those associated with the average compositions \bar{x}_{CO_2} or \bar{y}_{CO_2} .

Details about the methodology for describing and calculating the propagation of the uncertainty in the measured variables T , p , x_{CO_2} and y_{CO_2} into resulting estimates associated with each composition sample are given in [1], and the symbols used are summarized in Table S.1 in the Supplementary Material together with the data for the individual composition samples.

The propagation of uncertainty from the data of an individual sample, \bar{T} , \bar{p} , x_{CO_2} or y_{CO_2} , into the mean values for a series of samples, \bar{T}_f , \bar{p}_f , \bar{x}_{CO_2} or \bar{y}_{CO_2} , is defined by Eqs. (11)-(14) in [1], and the symbols are defined in the footnotes of Tables 7, 8 and 9.

4. Results

VLE measurements at the average temperatures 218.15, 233.14, 253.15, 273.15, 288.14 and 298.14 K were conducted, spanning from close to the triple point temperature (216.59 K) to close to the critical temperature of CO₂ (304.13 K), and covered pressures from the vapor pressure of CO₂ up to close to the critical point at each temperature.

The temperature \bar{T} , pressure \bar{p} and mole fractions for the liquid phase x_{CO_2} and the vapor phase y_{CO_2} for each individual sample are given in Tables S.2 and S.3 in the Supplementary Material, together with their uncertainty estimates. The composition derivatives with respect to pressure, $\partial x_{\text{CO}_2}/\partial p$ and $\partial y_{\text{CO}_2}/\partial p$, and the total standard uncertainties in the composition of the samples, $u_{\text{tot}}(x_{\text{CO}_2})$ and $u_{\text{tot}}(y_{\text{CO}_2})$, which were calculated using the scaling law in Section 5.3, are identified in Tables S.2 and S.3 in the Supplementary Material using the marker symbol ⁺.

The data for each series of samples are given at mean temperature \bar{T}_f , mean pressure \bar{p}_f and mean mole fractions for the liquid phase \bar{x}_{CO_2} and the vapor phase \bar{y}_{CO_2} in Tables 7 and 8. These averaged data are plotted with the uncertainties in composition and pressure in Figs. 5a to 5f. The relative volatilities based on the measured data are plotted in Figs S.1a to S.1f in the Supplementary Material. The means of the total standard uncertainties of the mole fractions, $\bar{u}_{\text{tot}}(x_{\text{CO}_2})$ and $\bar{u}_{\text{tot}}(y_{\text{CO}_2})$, and the final standard uncertainties of the mole fractions, $u_c(\bar{x}_{\text{CO}_2})$ and $u_c(\bar{y}_{\text{CO}_2})$, which were calculated using the scaling law in Section 5.3, are identified in Tables 7 and 8 using the marker symbol ⁺.

As discussed in Section 2.3.2, a special procedure was used to obtain VLE measurements close to the critical point at the temperatures 218.15, 233.14, 253.15 and 273.15 K. Four pressure-temperature-composition state points in the supercritical region were obtained, consisting of 4 pairs of composition sample series taken using both the liquid and vapor phase samplers. The individual sample data are given in Table S.4 in the Supplementary Material, and the average values for each series can be found in Table 9. The VLE points obtained using this procedure are identified in Tables S.2 and S.3 in the Supplementary Material, and in Tables 7 and 8. These VLE and supercritical measurements will be discussed in detail in Section 5.3.

5. Analysis and discussion

5.1. Summary and analysis of uncertainty estimates

With reference to Table 7, the maximum and average sample standard deviation of the liquid phase mole fractions,

Table 7

Liquid phase: Experimental VLE data for CO₂ (1) + O₂ (2) at mean temperature \bar{T}_f , mean pressure \bar{p}_f , and mean liquid phase mole fraction \bar{x}_{CO_2} ^a.

| ID | Data | | | Temperature | | | Pressure | | | Composition | | | |
|------|--------------------|----------------------|--------------------------------|-----------------------|-------------------------------|-------------------------|-------------------------|---------------------------------|---------------------------|-----------------------------------|--|-------------------------------------|--------------------------------------|
| | \bar{T}_f (K) | \bar{p}_f (MPa) | \bar{x}_{CO_2} (-) | $s(\bar{T}_f)$ (K) | $\bar{u}_c(\bar{T}_f)$ (K) | $u_c(\bar{T}_f)$ (K) | $s(\bar{p}_f)$ (MPa) | $\bar{u}_c(\bar{p}_f)$ (MPa) | $u_c(\bar{p}_f)$ (MPa) | $s(\bar{x}_{\text{CO}_2})$ (-) | $\bar{u}_{\text{tot}}(x_{\text{CO}_2})$ (-) | $u_c(\bar{x}_{\text{CO}_2})$ (-) | $x_{\text{CO}_2,\text{calc}}$ (-) |
| P1 | 218.147 | 0.5546 ^b | 0.99999 | 7.3e-5 | 3.7e-3 | 3.7e-3 | 1.1e-6 | 4.9e-4 | 4.9e-4 | | | | |
| L1 | 218.148 | 2.1957 | 0.96687 | 2.0e-4 | 3.5e-3 | 3.5e-3 | 9.5e-6 | 5.2e-4 | 5.2e-4 | 4.8e-6 | 4.8e-4 | 4.8e-4 | 0.96887 |
| L2 | 218.148 | 3.9362 | 0.92958 | 7.8e-5 | 3.7e-3 | 3.7e-3 | 1.9e-5 | 1.1e-3 | 1.1e-3 | 3.8e-6 | 4.8e-4 | 4.8e-4 | 0.93250 |
| L3 | 218.148 | 5.9189 | 0.88226 | 4.3e-4 | 3.4e-3 | 3.4e-3 | 6.8e-6 | 1.1e-3 | 1.1e-3 | 3.5e-6 | 4.8e-4 | 4.8e-4 | 0.88563 |
| L4 | 218.149 | 7.8935 | 0.82832 | 1.7e-4 | 3.5e-3 | 3.5e-3 | 5.0e-6 | 1.2e-3 | 1.2e-3 | 4.8e-6 | 4.8e-4 | 4.8e-4 | 0.83104 |
| L5 | 218.148 | 9.7335 | 0.76941 | 9.8e-5 | 3.4e-3 | 3.4e-3 | 5.5e-6 | 1.4e-3 | 1.4e-3 | 3.0e-6 | 4.8e-4 | 4.8e-4 | 0.76955 |
| L6 | 218.148 | 11.7910 | 0.68723 | 1.3e-4 | 3.5e-3 | 3.5e-3 | 1.0e-5 | 2.7e-3 | 2.7e-3 | 5.3e-6 | 5.0e-4 | 5.0e-4 | 0.67972 |
| L7 | 218.148 | 13.0212 | 0.61994 | 1.4e-4 | 3.5e-3 | 3.5e-3 | 1.3e-5 | 2.8e-3 | 2.8e-3 | 7.2e-6 | 5.2e-4 | 5.2e-4 | 0.60470 |
| L8 | 218.148 | 14.0358 | 0.53329 | 1.6e-4 | 3.6e-3 | 3.6e-3 | 2.0e-5 | 2.8e-3 | 2.8e-3 | 2.5e-5 | 6.0e-4 ⁺ | 6.0e-4 ⁺ | 0.51002 |
| L9* | 218.148 | 14.3563 | 0.47535 | 1.2e-4 | 3.3e-3 | 3.3e-3 | 1.3e-5 | 2.8e-3 | 2.8e-3 | 5.0e-6 | 9.8e-4 ⁺ | 9.8e-4 ⁺ | 0.45826 |
| L10* | 218.148 | 14.3873 | 0.46440 | 1.2e-4 | 3.4e-3 | 3.4e-3 | 1.7e-5 | 2.8e-3 | 2.8e-3 | 5.4e-6 | 1.3e-3 ⁺ | 1.3e-3 ⁺ | 0.45116 |
| L11* | 218.149 | 14.4111 | 0.45232 | 2.1e-4 | 3.3e-3 | 3.3e-3 | 1.6e-5 | 2.8e-3 | 2.8e-3 | 2.4e-5 | 1.9e-3 ⁺ | 1.9e-3 ⁺ | 0.44512 |
| P2 | 233.143 | 1.0048 ^c | 0.99999 | 7.4e-5 | 6.8e-3 | 6.8e-3 | 1.1e-5 | 5.1e-4 | 5.1e-4 | | | | |
| L13 | 233.142 | 1.9677 | 0.98023 | 1.1e-4 | 7.2e-3 | 7.2e-3 | 8.4e-6 | 5.1e-4 | 5.1e-4 | 8.9e-5 | 4.8e-4 | 4.9e-4 | 0.98262 |
| L14 | 233.141 | 2.9345 | 0.96020 | 5.5e-5 | 7.8e-3 | 7.8e-3 | 2.3e-5 | 5.3e-4 | 5.3e-4 | 4.4e-6 | 4.8e-4 | 4.8e-4 | 0.96410 |
| L15 | 233.143 | 3.9408 | 0.93829 | 2.3e-4 | 6.8e-3 | 6.8e-3 | 4.4e-5 | 1.1e-3 | 1.1e-3 | 4.6e-6 | 4.8e-4 | 4.8e-4 | 0.94358 |
| L16 | 233.143 | 5.9477 | 0.89067 | 2.6e-4 | 7.3e-3 | 7.3e-3 | 7.2e-6 | 1.1e-3 | 1.1e-3 | 3.0e-6 | 4.8e-4 | 4.8e-4 | 0.89803 |
| L17 | 233.143 | 7.8334 | 0.84017 | 2.0e-4 | 7.5e-3 | 7.5e-3 | 9.7e-6 | 1.2e-3 | 1.2e-3 | 3.5e-6 | 4.8e-4 | 4.8e-4 | 0.84775 |
| L18 | 233.142 | 8.8724 | 0.80939 | 6.0e-4 | 7.5e-3 | 7.5e-3 | 9.4e-6 | 1.3e-3 | 1.3e-3 | 1.8e-5 | 4.8e-4 | 4.8e-4 | 0.81577 |
| L19 | 233.142 | 9.8514 | 0.77736 | 3.3e-4 | 7.1e-3 | 7.1e-3 | 1.1e-5 | 1.4e-3 | 1.4e-3 | 8.9e-6 | 4.8e-4 | 4.8e-4 | 0.78187 |
| L20 | 233.140 | 11.8341 | 0.69897 | 1.5e-4 | 7.3e-3 | 7.3e-3 | 8.8e-6 | 2.7e-3 | 2.7e-3 | 4.8e-6 | 5.0e-4 | 5.0e-4 | 0.69628 |
| L21 | 233.142 | 12.8248 | 0.64711 | 1.2e-4 | 6.9e-3 | 6.9e-3 | 8.7e-6 | 2.7e-3 | 2.7e-3 | 7.7e-6 | 5.1e-4 | 5.1e-4 | 0.63897 |
| L22 | 233.142 | 13.6445 | 0.58762 | 5.2e-4 | 7.2e-3 | 7.2e-3 | 9.3e-6 | 2.8e-3 | 2.8e-3 | 7.4e-6 | 5.4e-4 ⁺ | 5.4e-4 ⁺ | 0.57569 |
| L23* | 233.144 | 14.1868 | 0.51081 | 7.8e-5 | 6.9e-3 | 6.9e-3 | 1.0e-5 | 2.8e-3 | 2.8e-3 | 3.2e-6 | 9.7e-4 ⁺ | 9.7e-4 ⁺ | 0.51244 |
| L24* | 233.144 | 14.2158 | 0.50044 | 9.6e-5 | 6.7e-3 | 6.7e-3 | 1.7e-5 | 2.8e-3 | 2.8e-3 | 4.4e-6 | 1.3e-3 ⁺ | 1.3e-3 ⁺ | 0.50771 |
| L25* | 233.146 | 14.2407 | 0.48640 | 2.5e-4 | 6.0e-3 | 6.0e-3 | 1.1e-5 | 2.8e-3 | 2.8e-3 | 4.3e-6 | 2.4e-3 ⁺ | 2.4e-3 ⁺ | 0.50339 |
| P3 | 253.147 | 1.9699 ^d | 0.99999 | 1.5e-5 | 5.7e-3 | 5.7e-3 | 5.5e-6 | 5.1e-4 | 5.1e-4 | | | | |
| L27 | 253.146 | 2.9632 | 0.97899 | 1.3e-4 | 5.8e-3 | 5.8e-3 | 2.9e-5 | 5.2e-4 | 5.2e-4 | 1.3e-5 | 4.8e-4 | 4.8e-4 | 0.98167 |
| L28 | 253.146 | 4.9365 | 0.93518 | 1.2e-4 | 6.0e-3 | 6.0e-3 | 9.4e-5 | 1.1e-3 | 1.1e-3 | 2.6e-6 | 4.8e-4 | 4.8e-4 | 0.94105 |
| L29 | 253.146 | 6.9081 | 0.88640 | 1.9e-4 | 6.0e-3 | 6.0e-3 | 4.4e-5 | 1.1e-3 | 1.1e-3 | 9.5e-6 | 4.8e-4 | 4.8e-4 | 0.89327 |
| L30 | 253.146 | 8.3058 | 0.84783 | 1.4e-4 | 5.9e-3 | 5.9e-3 | 1.3e-5 | 1.2e-3 | 1.2e-3 | 5.2e-6 | 4.8e-4 | 4.8e-4 | 0.85331 |
| L31 | 253.148 | 9.6226 | 0.80640 | 1.3e-4 | 5.7e-3 | 5.7e-3 | 3.9e-4 | 1.5e-3 | 1.5e-3 | 8.4e-6 | 4.8e-4 | 4.8e-4 | 0.80906 |
| L32 | 253.147 | 10.8463 | 0.76222 | 1.4e-4 | 5.8e-3 | 5.8e-3 | 4.3e-5 | 2.7e-3 | 2.7e-3 | 7.7e-6 | 4.9e-4 | 4.9e-4 | 0.75948 |
| L33 | 253.146 | 11.8557 | 0.71747 | 9.3e-5 | 6.0e-3 | 6.0e-3 | 2.5e-5 | 2.7e-3 | 2.7e-3 | 8.3e-6 | 5.0e-4 | 5.0e-4 | 0.70866 |
| L34 | 253.146 | 12.7678 | 0.66173 | 8.9e-5 | 5.7e-3 | 5.7e-3 | 3.6e-5 | 2.7e-3 | 2.7e-3 | 6.6e-6 | 5.2e-4 ⁺ | 5.2e-4 ⁺ | 0.64728 |
| L35* | 253.146 | 13.2762 | 0.59988 | 1.2e-4 | 5.7e-3 | 5.7e-3 | 1.7e-5 | 2.7e-3 | 2.7e-3 | 8.6e-6 | 8.8e-4 ⁺ | 8.8e-4 ⁺ | 0.59446 |
| L36* | 253.147 | 13.3024 | 0.59165 | 1.1e-4 | 5.8e-3 | 5.8e-3 | 1.8e-5 | 2.7e-3 | 2.7e-3 | 1.7e-5 | 1.1e-3 ⁺ | 1.1e-3 ⁺ | 0.59060 |
| L37* | 253.147 | 13.3201 | 0.58371 | 1.2e-4 | 5.8e-3 | 5.8e-3 | 5.7e-5 | 2.7e-3 | 2.7e-3 | 1.6e-5 | 1.6e-3 ⁺ | 1.6e-3 ⁺ | 0.58784 |
| P4 | 273.147 | 3.4848 ^e | 0.99999 | 2.4e-5 | 1.5e-3 | 1.5e-3 | 9.9e-7 | 1.1e-3 | 1.1e-3 | | | | |
| L39 | 273.145 | 5.0161 | 0.96558 | 8.5e-5 | 2.0e-3 | 2.0e-3 | 2.2e-5 | 1.1e-3 | 1.1e-3 | 3.0e-6 | 4.8e-4 | 4.8e-4 | 0.96828 |
| L40 | 273.146 | 5.9255 | 0.94385 | 1.6e-4 | 2.5e-3 | 2.5e-3 | 2.7e-5 | 1.1e-3 | 1.1e-3 | 3.1e-6 | 4.8e-4 | 4.8e-4 | 0.94709 |
| L41 | 273.146 | 6.9258 | 0.91829 | 6.8e-5 | 2.4e-3 | 2.4e-3 | 3.7e-5 | 1.1e-3 | 1.1e-3 | 2.7e-6 | 4.8e-4 | 4.8e-4 | 0.92127 |
| L42 | 273.146 | 7.9107 | 0.89110 | 1.2e-4 | 2.4e-3 | 2.4e-3 | 2.9e-5 | 1.2e-3 | 1.2e-3 | 6.6e-6 | 4.8e-4 | 4.8e-4 | 0.89260 |
| L43 | 273.146 | 8.8894 | 0.86113 | 9.3e-5 | 2.4e-3 | 2.4e-3 | 6.1e-5 | 1.3e-3 | 1.3e-3 | 1.4e-5 | 4.8e-4 | 4.8e-4 | 0.85979 |
| L44 | 273.145 | 9.8537 | 0.82710 | 1.8e-4 | 2.4e-3 | 2.4e-3 | 1.5e-4 | 1.4e-3 | 1.4e-3 | 6.3e-6 | 4.8e-4 | 4.8e-4 | 0.82128 |
| L45 | 273.147 | 10.8864 | 0.78003 | 6.0e-5 | 2.4e-3 | 2.4e-3 | 1.6e-5 | 2.7e-3 | 2.7e-3 | 6.8e-5 | 5.1e-4 | 5.1e-4 | 0.76737 |
| L46 | 273.146 | 11.3314 | 0.74899 | 8.2e-5 | 2.3e-3 | 2.3e-3 | 1.2e-4 | 2.7e-3 | 2.7e-3 | 2.8e-5 | 5.4e-4 ⁺ | 5.4e-4 ⁺ | 0.73428 |
| L47* | 273.145 | 11.5579 | 0.71514 | 2.5e-4 | 2.6e-3 | 2.6e-3 | 1.5e-5 | 2.7e-3 | 2.7e-3 | 1.6e-5 | 1.1e-3 ⁺ | 1.1e-3 ⁺ | 0.70945 |
| L48* | 273.146 | 11.5779 | 0.70363 | 1.7e-4 | 2.3e-3 | 2.3e-3 | 6.6e-6 | 2.7e-3 | 2.7e-3 | 1.3e-4 | 3.0e-3 ⁺ | 3.0e-3 ⁺ | 0.70648 |
| P5 | 288.139 | 5.0859 ^f | 0.99999 | 2.8e-4 | 1.8e-3 | 1.8e-3 | 2.9e-6 | 1.1e-3 | 1.1e-3 | | | | |
| L50 | 288.137 | 5.6498 | 0.98649 | 9.1e-4 | 1.7e-3 | 2.0e-3 | 1.3e-5 | 1.1e-3 | 1.1e-3 | 2.0e-5 | 4.8e-4 | 4.8e-4 | 0.98744 |
| L51 | 288.136 | 7.0494 | 0.95060 | 4.2e-4 | 1.6e-3 | 1.6e-3 | 7.5e-6 | 1.1e-3 | 1.1e-3 | 1.3e-6 | 4.8e-4 | 4.8e-4 | 0.95110 |
| L52 | 288.134 | 8.4289 | 0.90854 | 6.8e-4 | 1.6e-3 | 1.7e-3 | 9.2e-6 | 1.2e-3 | 1.2e-3 | 1.8e-6 | 4.8e-4 | 4.8e-4 | 0.90541 |
| L53 | 288.137 | 8.8666 | 0.89230 | 9.0e-4 | 1.7e-3 | 1.9e-3 | 1.7e-6 | 1.3e-3 | 1.3e-3 | 4.4e-6 | 4.8e-4 | 4.8e-4 | 0.88720 |
| L54 | 288.138 | 9.2573 | 0.87508 | 1.7e-4 | 1.6e-3 | 1.6e-3 | 1.1e-5 | 1.3e-3 | 1.3e-3 | 6.1e-6 | 4.8e-4 | 4.8e-4 | 0.86795 |
| L55 | 288.139 | 9.5784 | 0.85590 | 9.8e-4 | 1.8e-3 | 2.1e-3 | 1.0e-5 | 1.4e-3 | 1.4e-3 | 5.2e-6 | 4.9e-4 ⁺ | 4.9e-4 ⁺ | 0.84786 |
| L56 | 288.138 | 9.7066 | 0.84282 | 1.2e-3 | 1.7e-3 | 2.1e-3 | 2.6e-5 | 1.4e-3 | 1.4e-3 | 5.2e-6 | 5.2e-4 ⁺ | 5.2e-4 ⁺ | 0.83726 |
| L57 | 288.141 | 9.7231 | 0.84006 | 4.2e-5 | 1.8e-3 | 1.8e-3 | 1.3e-5 | 1.4e-3 | 1.4e-3 | 3.5e-6 | 5.5e-4 ⁺ | 5.5e-4 ⁺ | 0.83565 |
| L58 | 288.139 | 9.7447 | 0.83495 | 1.5e-3 | 1.9e-3 | 2.4e-3 | 8.7e-6 | 1.4e-3 | 1.4e-3 | 2.6e-5 | 6.6e-4 ⁺ | 6.6e-4 ⁺ | 0.83343 |
| P6 | 298.137 | 6.4328 ^g | 0.99999 | 1.1e-4 | 3.0e-3 | 3.0e-3 | 8.6e-6 | 1.1e-3 | 1.1e-3 | | | | |
| L59 | 298.133 | 7.1110 | 0.98137 | 6.6e-4 | 3.0e-3 | 3.1e-3 | 6.5e-6 | 1.1e-3 | 1.1e-3 | 1.1e-6 | 4.8e-4 | 4.8e-4 | 0.98158 |
| L60 | 298.135 | 7.4191 | 0.97218 | 5.0e-4 | 3.1e-3 | 3.2e-3 | 5.0e-6 | 1.1e-3 | 1.1e-3 | 7.0e-7 | 4.8e-4 | 4.8e-4 | 0.97195 |
| L61 | 298.134 | 7.8403 | 0.95809 | 1.0e-3 | 3.0e-3 | 3.1e-3 | 1.1e-4 | 1.1e-3 | 1.2e-3 | 2.3e-6 | 4.8e-4 | 4.8e-4 | 0.95692 |
| L62 | 298.135 | 8.0258 | 0.95087 | 1.4e-3 | 3.2e-3 | 3.5e-3 | 7.7e-6 | 1.1e-3 | 1.1e-3 | 2.7e-6 | 4.8e-4 | 4.8e-4 | 0.94920 |
| L63 | 298.135 | 8.1284 | 0.94625 | 2.6e-4 | 3.0e-3 | 3.0e-3 | 9.6e-6 | 1.2e-3 | 1.2e-3 | 1.0e-6 | 4.8e-4 | 4.8e-4 | 0.94443 |
| L64 | 298.135 | 8.2648 | 0.93815 | 2.3e-4 | 3.2e-3 | 3.2e-3 | 9.7e-6 | 1.2e-3 | 1.2e-3 | 1.5e-6 | 4.9e-4 ⁺ | 4.9e-4 ⁺ | 0.93709 |
| L65 | 298.136 | 8.3019 | 0.93439 | 5.1e-4 | 3.3e-3 | 3.3e-3 | 1.0e-5 | 1.2e-3 | 1.2e-3 | 5.2e-6 | 5.1e-4 ⁺ | 5.1e-4 ⁺ | 0.93474 |
| L66 | 298.134 | 8.3180 | 0.93085 | 4.1e-4 | 3.1e-3 | 3.2e-3 | 4.5e-6 | 1.2e-3 | 1.2e-3 | 2.8e-5 | 7.2e-4 ⁺ | 7.2e-4 ⁺ | 0.93363 |

^a Sample standard deviation of the mean of the temperatures $s(\bar{T}_f)$, mean of the standard systematic uncertainty of the temperatures $\bar{u}_c(\bar{T}_f)$, total standard uncertainty of the temperature $u_c(\bar{T}_f)$, sample standard deviation of the mean of the pressures $s(\bar{p}_f)$, mean of the standard systematic uncertainty of the pressures $\bar{u}_c(\bar{p}_f)$, total standard uncertainty of the pressure $u_c(\bar{p}_f)$, sample standard deviation of the mean of the mole fractions $s(\bar{x}_{\text{CO}_2})$, mean of the total standard uncertainty of the mole fractions $\bar{u}_{\text{tot}}(x_{\text{CO}_2})$, final standard uncertainty of the mole fraction $u_c(\bar{x}_{\text{CO}_2})$, PR-MC-WS-NRTL Case 2 EOS calculated mole fraction $x_{\text{CO}_2,\text{calc}}(\bar{T}_f, \bar{p}_f)$ ^b Span-Wagner CO₂ vapor pressure is 0.5539 ± 0.0002 MPa.

^c Span-Wagner CO₂ vapor pressure is 1.0042 ± 0.0003 MPa. ^d Span-Wagner CO₂ vapor pressure is 1.9694 ± 0.0006 MPa. ^e Span-Wagner CO₂ vapor pressure is 3.4849 ± 0.0010 MPa.

^f Span-Wagner CO₂ vapor pressure is 5.0859 ± 0.0015 MPa. ^g Span-Wagner CO₂ vapor pressure is 6.4324 ± 0.0019 MPa. ^h Measured together with the supercritical data in Table 9 using the procedure in Section 2.3.2.

⁺ The derivatives $\partial x_{\text{CO}_2} / \partial p$ used in Eq. (5) to obtain $\bar{u}_{\text{tot}}(x_{\text{CO}_2})$ were calculated using the scaling law in Eq. (6) with the parameters in Table 11 instead of the PR-MC-WS-NRTL Case 2 fitted EOS. See Table S.2 in the Supplementary Material for the values of the derivatives, and Section 5.3 for details.

Table 8

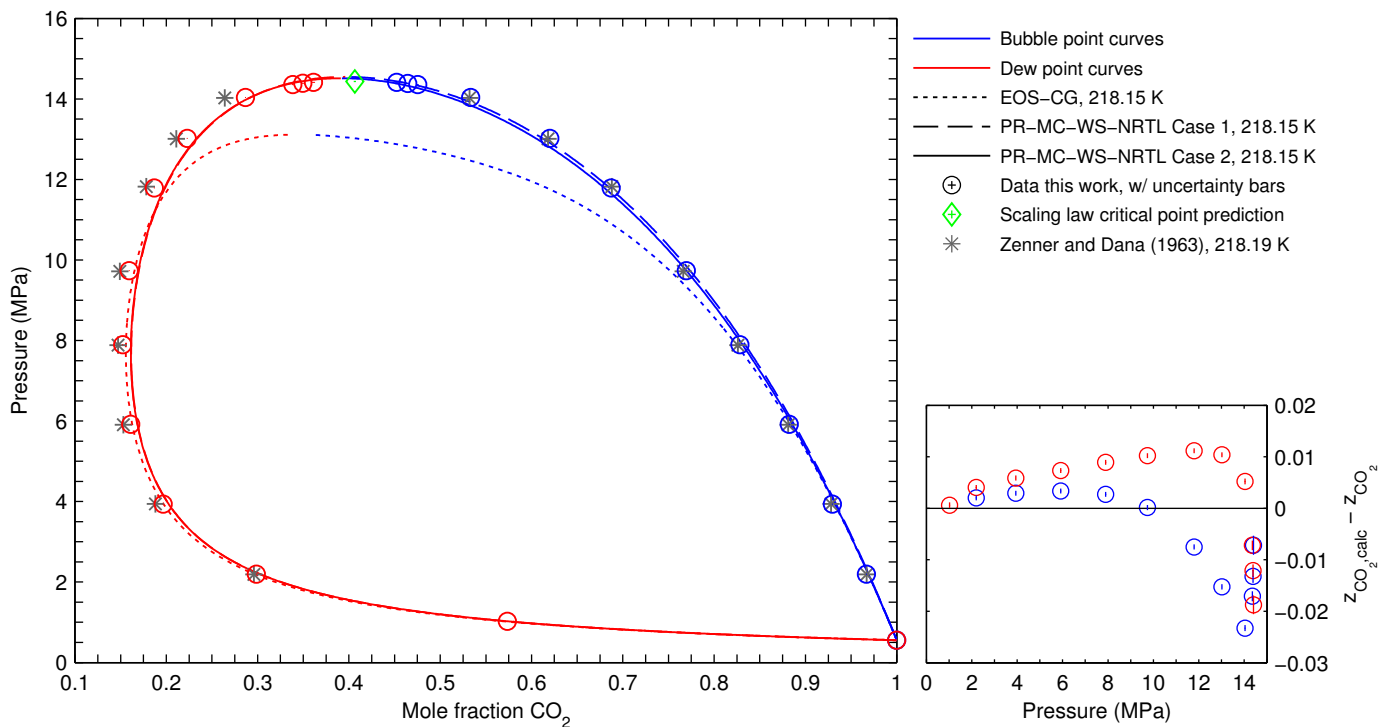
Vapor phase: Experimental VLE data for CO₂ (1) + O₂ (2) at mean temperature \bar{T}_f , mean pressure \bar{p}_f , and mean vapor phase mole fraction \bar{y}_{CO_2} ^a.

| ID | Data | | | Temperature | | | Pressure | | | Composition | | | |
|------------------|--------------------|----------------------|--------------------------------|-----------------------|-----------------------------|-------------------------|-------------------------|-------------------------------|---------------------------|-----------------------------------|--|-------------------------------|--------------------------------------|
| | \bar{T}_f (K) | \bar{p}_f (MPa) | \bar{y}_{CO_2} (-) | $s(\bar{T}_f)$ (K) | $\bar{u}_c(\bar{T})$ (K) | $u_c(\bar{T}_f)$ (K) | $s(\bar{p}_f)$ (MPa) | $\bar{u}_c(\bar{p})$ (MPa) | $u_c(\bar{p}_f)$ (MPa) | $s(\bar{y}_{\text{CO}_2})$ (-) | $\bar{u}_{\text{tot}}(y_{\text{CO}_2})$ (-) | $u_c(y_{\text{CO}_2})$ (-) | $y_{\text{CO}_2,\text{calc}}$ (-) |
| P1 | 218.147 | 0.5546 ^b | 0.99999 | 7.3e-5 | 3.7e-3 | 3.7e-3 | 1.1e-6 | 4.9e-4 | 4.9e-4 | | | | |
| V1 | 218.148 | 1.0237 | 0.57354 | 6.1e-5 | 3.4e-3 | 3.4e-3 | 3.6e-5 | 5.1e-4 | 5.1e-4 | 1.0e-4 | 5.5e-4 | 5.6e-4 | 0.57416 |
| V2 | 218.148 | 2.1957 | 0.29849 | 2.0e-4 | 3.5e-3 | 3.5e-3 | 1.6e-5 | 5.2e-4 | 5.2e-4 | 5.0e-5 | 4.8e-4 | 4.9e-4 | 0.30252 |
| V3 | 218.148 | 3.9362 | 0.19663 | 4.8e-5 | 3.8e-3 | 3.8e-3 | 1.1e-5 | 1.1e-3 | 1.1e-3 | 4.2e-5 | 4.8e-4 | 4.8e-4 | 0.20251 |
| V4 | 218.150 | 5.9189 | 0.16093 | 7.3e-5 | 3.2e-3 | 3.2e-3 | 4.7e-6 | 1.1e-3 | 1.1e-3 | 1.4e-5 | 4.8e-4 | 4.8e-4 | 0.16826 |
| V5 | 218.148 | 7.8935 | 0.15229 | 2.4e-4 | 3.5e-3 | 3.5e-3 | 5.9e-6 | 1.2e-3 | 1.2e-3 | 1.1e-5 | 4.8e-4 | 4.8e-4 | 0.16120 |
| V6 | 218.148 | 9.7335 | 0.15918 | 1.1e-4 | 3.5e-3 | 3.5e-3 | 8.1e-6 | 1.4e-3 | 1.4e-3 | 7.2e-6 | 4.8e-4 | 4.8e-4 | 0.16940 |
| V7 | 218.147 | 11.7910 | 0.18681 | 1.7e-4 | 3.5e-3 | 3.5e-3 | 1.1e-5 | 2.7e-3 | 2.7e-3 | 5.6e-6 | 4.8e-4 | 4.8e-4 | 0.19797 |
| V8 | 218.148 | 13.0211 | 0.22283 | 1.4e-4 | 3.5e-3 | 3.5e-3 | 1.6e-5 | 2.8e-3 | 2.8e-3 | 8.8e-6 | 4.9e-4 | 4.9e-4 | 0.23321 |
| V9 | 218.148 | 14.0359 | 0.28665 | 2.0e-4 | 3.6e-3 | 3.6e-3 | 2.2e-5 | 2.8e-3 | 2.8e-3 | 3.8e-5 | 5.7e-4 ⁺ | 5.7e-4 ⁺ | 0.29187 |
| V10 [*] | 218.148 | 14.3563 | 0.33855 | 4.8e-5 | 3.2e-3 | 3.2e-3 | 9.5e-6 | 2.8e-3 | 2.8e-3 | 1.7e-5 | 9.4e-4 ⁺ | 9.4e-4 ⁺ | 0.33136 |
| V11 [*] | 218.147 | 14.3873 | 0.34936 | 2.0e-4 | 3.3e-3 | 3.3e-3 | 7.4e-6 | 2.8e-3 | 2.8e-3 | 2.0e-5 | 1.2e-3 ⁺ | 1.2e-3 ⁺ | 0.33726 |
| V12 [*] | 218.149 | 14.4111 | 0.36111 | 1.9e-4 | 3.3e-3 | 3.3e-3 | 1.5e-5 | 2.8e-3 | 2.8e-3 | 7.5e-5 | 1.8e-3 ⁺ | 1.8e-3 ⁺ | 0.34237 |
| P2 | 233.143 | 1.0048 ^c | 0.99999 | 7.4e-5 | 6.8e-3 | 6.8e-3 | 1.1e-5 | 5.1e-4 | 5.1e-4 | | | | |
| V14 | 233.142 | 1.9677 | 0.56397 | 1.5e-4 | 7.3e-3 | 7.3e-3 | 2.3e-6 | 5.1e-4 | 5.1e-4 | 1.2e-4 | 5.1e-4 | 5.3e-4 | 0.56621 |
| V15 | 233.142 | 2.9346 | 0.41117 | 2.1e-4 | 7.7e-3 | 7.7e-3 | 1.3e-5 | 5.2e-4 | 5.3e-4 | 3.3e-5 | 4.9e-4 | 4.9e-4 | 0.41571 |
| V16 | 233.143 | 3.9408 | 0.33185 | 3.1e-4 | 6.8e-3 | 6.8e-3 | 2.5e-5 | 1.1e-3 | 1.1e-3 | 1.4e-5 | 4.9e-4 | 4.9e-4 | 0.33997 |
| V17 | 233.143 | 5.9475 | 0.26280 | 7.5e-5 | 7.6e-3 | 7.6e-3 | 9.5e-5 | 1.1e-3 | 1.1e-3 | 4.7e-6 | 4.8e-4 | 4.8e-4 | 0.27331 |
| V18 | 233.142 | 7.8335 | 0.24021 | 2.3e-4 | 7.5e-3 | 7.5e-3 | 3.5e-6 | 1.2e-3 | 1.2e-3 | 2.0e-5 | 4.8e-4 | 4.8e-4 | 0.25240 |
| V19 | 233.141 | 8.8724 | 0.23715 | 3.2e-4 | 7.6e-3 | 7.6e-3 | 4.4e-6 | 1.3e-3 | 1.3e-3 | 2.2e-5 | 4.8e-4 | 4.8e-4 | 0.25033 |
| V20 | 233.141 | 9.8514 | 0.23940 | 1.1e-4 | 7.5e-3 | 7.5e-3 | 7.7e-6 | 1.4e-3 | 1.4e-3 | 5.4e-6 | 4.8e-4 | 4.8e-4 | 0.25343 |
| V21 | 233.141 | 11.8341 | 0.26143 | 1.6e-4 | 7.2e-3 | 7.2e-3 | 9.4e-6 | 2.7e-3 | 2.7e-3 | 1.0e-5 | 4.8e-4 | 4.8e-4 | 0.27633 |
| V22 | 233.142 | 12.8248 | 0.28657 | 2.0e-4 | 7.2e-3 | 7.2e-3 | 1.1e-5 | 2.7e-3 | 2.7e-3 | 1.3e-5 | 4.9e-4 | 4.9e-4 | 0.30036 |
| V23 | 233.142 | 13.6445 | 0.32548 | 1.6e-4 | 7.3e-3 | 7.3e-3 | 7.4e-6 | 2.7e-3 | 2.7e-3 | 1.5e-5 | 5.2e-4 ⁺ | 5.2e-4 ⁺ | 0.33416 |
| V24 [*] | 233.144 | 14.1868 | 0.39244 | 2.0e-4 | 6.8e-3 | 6.8e-3 | 1.5e-5 | 2.8e-3 | 2.8e-3 | 2.8e-5 | 9.4e-4 ⁺ | 9.4e-4 ⁺ | 0.37661 |
| V25 [*] | 233.144 | 14.2158 | 0.40299 | 3.9e-4 | 6.6e-3 | 6.6e-3 | 7.2e-6 | 2.8e-3 | 2.8e-3 | 2.7e-5 | 1.3e-3 ⁺ | 1.3e-3 ⁺ | 0.38020 |
| V26 [*] | 233.145 | 14.2407 | 0.41751 | 1.2e-4 | 6.0e-3 | 6.0e-3 | 1.1e-5 | 2.8e-3 | 2.8e-3 | 1.1e-5 | 2.4e-3 ⁺ | 2.4e-3 ⁺ | 0.38354 |
| P3 | 253.147 | 1.9699 ^d | 0.99999 | 1.5e-5 | 5.7e-3 | 5.7e-3 | 5.5e-6 | 5.1e-4 | 5.1e-4 | | | | |
| V28 | 253.147 | 2.9631 | 0.72731 | 8.7e-5 | 5.7e-3 | 5.7e-3 | 6.3e-5 | 5.3e-4 | 5.3e-4 | 9.5e-6 | 5.0e-4 | 5.0e-4 | 0.73135 |
| V29 | 253.146 | 4.9363 | 0.51051 | 7.5e-5 | 5.7e-3 | 5.7e-3 | 1.5e-5 | 1.1e-3 | 1.1e-3 | 2.2e-5 | 4.9e-4 | 4.9e-4 | 0.51935 |
| V30 | 253.146 | 6.9080 | 0.42654 | 1.6e-4 | 5.9e-3 | 5.9e-3 | 9.4e-6 | 1.1e-3 | 1.1e-3 | 2.7e-5 | 4.8e-4 | 4.8e-4 | 0.43955 |
| V31 | 253.146 | 8.3057 | 0.39990 | 1.8e-4 | 5.9e-3 | 5.9e-3 | 1.1e-5 | 1.2e-3 | 1.2e-3 | 1.1e-5 | 4.8e-4 | 4.8e-4 | 0.41507 |
| V32 | 253.148 | 9.6222 | 0.39110 | 6.1e-5 | 5.8e-3 | 5.8e-3 | 2.2e-5 | 1.4e-3 | 1.4e-3 | 8.6e-5 | 4.8e-4 | 4.9e-4 | 0.40751 |
| V33 | 253.148 | 10.8461 | 0.39517 | 2.1e-4 | 5.6e-3 | 5.6e-3 | 2.3e-4 | 2.7e-3 | 2.7e-3 | 1.5e-5 | 4.8e-4 | 4.8e-4 | 0.41263 |
| V34 | 253.146 | 11.8558 | 0.41081 | 6.8e-5 | 5.8e-3 | 5.8e-3 | 4.8e-5 | 2.7e-3 | 2.7e-3 | 1.2e-5 | 4.9e-4 | 4.9e-4 | 0.42773 |
| V35 | 253.146 | 12.7677 | 0.44495 | 1.4e-4 | 5.7e-3 | 5.7e-3 | 8.4e-6 | 2.7e-3 | 2.7e-3 | 5.7e-6 | 5.2e-4 ⁺ | 5.2e-4 ⁺ | 0.45666 |
| V36 [*] | 253.146 | 13.2762 | 0.50132 | 3.5e-4 | 5.8e-3 | 5.8e-3 | 4.2e-5 | 2.7e-3 | 2.7e-3 | 1.6e-5 | 8.6e-4 ⁺ | 8.6e-4 ⁺ | 0.49109 |
| V37 [*] | 253.147 | 13.3023 | 0.50988 | 1.2e-4 | 6.0e-3 | 6.0e-3 | 2.2e-5 | 2.7e-3 | 2.7e-3 | 6.0e-5 | 1.1e-3 ⁺ | 1.1e-3 ⁺ | 0.49401 |
| V38 [*] | 253.147 | 13.3200 | 0.51743 | 5.8e-5 | 5.8e-3 | 5.8e-3 | 6.6e-6 | 2.7e-3 | 2.7e-3 | 1.1e-5 | 1.6e-3 ⁺ | 1.6e-3 ⁺ | 0.49612 |
| P4 | 273.147 | 3.4848 ^e | 0.99999 | 2.4e-5 | 1.5e-3 | 1.5e-3 | 9.9e-7 | 1.1e-3 | 1.1e-3 | | | | |
| V40 | 273.144 | 3.9433 | 0.91844 | 1.3e-4 | 2.2e-3 | 2.2e-3 | 1.7e-5 | 1.1e-3 | 1.1e-3 | 1.1e-4 | 5.1e-4 | 5.2e-4 | 0.92150 |
| V41 | 273.145 | 5.0162 | 0.78625 | 2.1e-4 | 2.1e-3 | 2.1e-3 | 4.9e-5 | 1.1e-3 | 1.1e-3 | 3.6e-5 | 4.9e-4 | 4.9e-4 | 0.79225 |
| V42 | 273.146 | 5.9256 | 0.71346 | 6.1e-5 | 2.5e-3 | 2.5e-3 | 2.5e-5 | 1.1e-3 | 1.1e-3 | 1.2e-5 | 4.9e-4 | 4.9e-4 | 0.72173 |
| V43 | 273.146 | 6.9259 | 0.65904 | 8.1e-5 | 2.2e-3 | 2.2e-3 | 5.2e-5 | 1.1e-3 | 1.1e-3 | 1.2e-5 | 4.8e-4 | 4.8e-4 | 0.66945 |
| V44 | 273.146 | 7.9107 | 0.62377 | 2.4e-4 | 2.3e-3 | 2.3e-3 | 5.1e-5 | 1.2e-3 | 1.2e-3 | 1.1e-5 | 4.8e-4 | 4.8e-4 | 0.63597 |
| V45 | 273.146 | 8.8896 | 0.60275 | 9.9e-5 | 2.3e-3 | 2.3e-3 | 8.9e-5 | 1.3e-3 | 1.3e-3 | 1.0e-5 | 4.8e-4 | 4.8e-4 | 0.61637 |
| V46 | 273.146 | 9.8539 | 0.59503 | 1.5e-4 | 2.5e-3 | 2.5e-3 | 2.0e-5 | 1.4e-3 | 1.4e-3 | 5.3e-6 | 4.8e-4 | 4.8e-4 | 0.60925 |
| V47 | 273.146 | 10.8864 | 0.60684 | 1.7e-4 | 2.7e-3 | 2.7e-3 | 1.8e-5 | 2.7e-3 | 2.7e-3 | 7.8e-6 | 4.8e-4 | 4.8e-4 | 0.61857 |
| V48 | 273.146 | 11.3312 | 0.62764 | 9.4e-5 | 2.4e-3 | 2.4e-3 | 1.7e-5 | 2.7e-3 | 2.7e-3 | 2.6e-5 | 5.3e-4 ⁺ | 5.4e-4 ⁺ | 0.63335 |
| V49 [*] | 273.145 | 11.5578 | 0.66096 | 2.5e-5 | 2.6e-3 | 2.6e-3 | 2.3e-5 | 2.7e-3 | 2.7e-3 | 1.8e-5 | 1.1e-3 ⁺ | 1.1e-3 ⁺ | 0.64900 |
| V50 [*] | 273.146 | 11.5780 | 0.67276 | 1.3e-4 | 2.4e-3 | 2.4e-3 | 1.5e-5 | 2.7e-3 | 2.7e-3 | 9.9e-5 | 3.1e-3 ⁺ | 3.1e-3 ⁺ | 0.65119 |
| P5 | 288.139 | 5.0859 ^f | 0.99999 | 2.8e-4 | 1.8e-3 | 1.8e-3 | 2.9e-6 | 1.1e-3 | 1.1e-3 | | | | |
| V52 | 288.137 | 5.6498 | 0.94168 | 8.5e-4 | 1.7e-3 | 1.9e-3 | 3.5e-6 | 1.1e-3 | 1.1e-3 | 2.6e-5 | 4.9e-4 | 4.9e-4 | 0.94516 |
| V53 | 288.142 | 7.0493 | 0.84273 | 2.1e-5 | 1.8e-3 | 1.8e-3 | 6.8e-6 | 1.1e-3 | 1.1e-3 | 3.7e-5 | 4.8e-4 | 4.8e-4 | 0.84963 |
| V54 | 288.141 | 8.4289 | 0.79080 | 1.3e-3 | 1.8e-3 | 2.3e-3 | 1.4e-5 | 1.2e-3 | 1.2e-3 | 2.4e-5 | 4.8e-4 | 4.8e-4 | 0.79918 |
| V55 | 288.137 | 8.8666 | 0.78344 | 5.1e-4 | 1.8e-3 | 1.8e-3 | 2.3e-5 | 1.3e-3 | 1.3e-3 | 1.7e-6 | 4.8e-4 | 4.8e-4 | 0.79132 |
| V56 | 288.139 | 9.2573 | 0.78234 | 5.5e-4 | 1.7e-3 | 1.8e-3 | 8.7e-6 | 1.3e-3 | 1.3e-3 | 1.2e-6 | 4.8e-4 | 4.8e-4 | 0.78870 |
| V57 | 288.138 | 9.5784 | 0.78942 | 4.3e-4 | 1.7e-3 | 1.8e-3 | 1.2e-5 | 1.4e-3 | 1.4e-3 | 2.8e-6 | 4.9e-4 ⁺ | 4.9e-4 ⁺ | 0.79159 |
| V58 | 288.141 | 9.7066 | 0.79944 | 1.1e-4 | 1.7e-3 | 1.7e-3 | 2.0e-5 | 1.4e-3 | 1.4e-3 | 8.5e-6 | 5.1e-4 ⁺ | 5.1e-4 ⁺ | 0.79558 |
| V59 | 288.141 | 9.7232 | 0.80207 | 4.1e-4 | 1.9e-3 | 1.9e-3 | 1.0e-5 | 1.4e-3 | 1.4e-3 | 9.5e-6 | 5.3e-4 ⁺ | 5.3e-4 ⁺ | 0.79633 |
| V60 | 288.142 | 9.7447 | 0.80674 | 2.9e-5 | 1.9e-3 | 1.9e-3 | 3.9e-6 | 1.4e-3 | 1.4e-3 | 7.8e-5 | 6.4e-4 ⁺ | 6.5e-4 ⁺ | 0.79746 |
| P6 | 298.137 | 6.4328 ^g | 0.99999 | 1.1e-4 | 3.0e-3 | 3.0e-3 | 8.6e-6 | 1.1e-3 | 1.1e-3 | | | | |
| V61 | 298.141 | 7.1110 | 0.95624 | 4.8e-5 | 3.2e-3 | 3.2e-3 | 2.8e-6 | 1.1e-3 | 1.1e-3 | 1.3e-5 | 4.8e-4 | 4.8e-4 | 0.95967 |
| V62 | 298.135 | 7.4191 | 0.94072 | 7.8e-4 | 3.2e-3 | 3.3e-3 | 4.1e-6 | 1.1e-3 | 1.1e-3 | 2.7e-6 | 4.8e-4 | 4.8e-4 | 0.94483 |
| V63 | 298.138 | 7.8392 | 0.92467 | 1.4e-3 | 3.1e-3 | 3.4e-3 | 1.4e-4 | 1.1e-3 | 1.1e-3 | 1.1e-5 | 4.8e-4 | 4.8e-4 | 0.92886 |
| V64 | 298.140 | 8.0258 | 0.91978 | 3.9e-5 | 3.3e-3 | 3.3e-3 | 3.9e-6 | 1.1e-3 | 1.1e-3 | 8.6e-6 | 4.8e-4 | 4.8e-4 | 0.92365 |
| V65 | 298.135 | 8.1339 | 0.91818 | 3.6e-4 | 3.0e-3 | 3.0e-3 | 6.7e-6 | 1.2e-3 | 1.2e-3 | 1.0e-5 | 4.8e-4 | 4.8e-4 | 0.92129 |
| V66 | 298.135 | 8.2648 | 0.91898 | 7.1e-4 | 3.1e-3 | 3.2e-3 | 3.8e-6 | 1.2e-3 | 1.2e-3 | 9.2e-7 | 4.8e-4 ⁺ | 4.8e-4 ⁺ | 0.91966 |
| V67 | 298.137 | 8.3019 | 0.92108 | 4.4e-4 | 3.2e-3 | 3.2e-3 | 9.0e-6 | 1.2e-3 | 1.2e-3 | 6.4e-6 | 4.9e-4 ⁺ | 4.9e-4 ⁺ | 0.91960 |
| V68 | 298.136 | 8.3180 | 0.92389 | 1.0e-3 | 3.1e-3 | 3.3e-3 | 6.0e-6 | 1.2e-3 | 1.2e-3 | 1.0e-5 | 6.9e-4 ⁺ | 6.9e-4 ⁺ | 0.91965 |

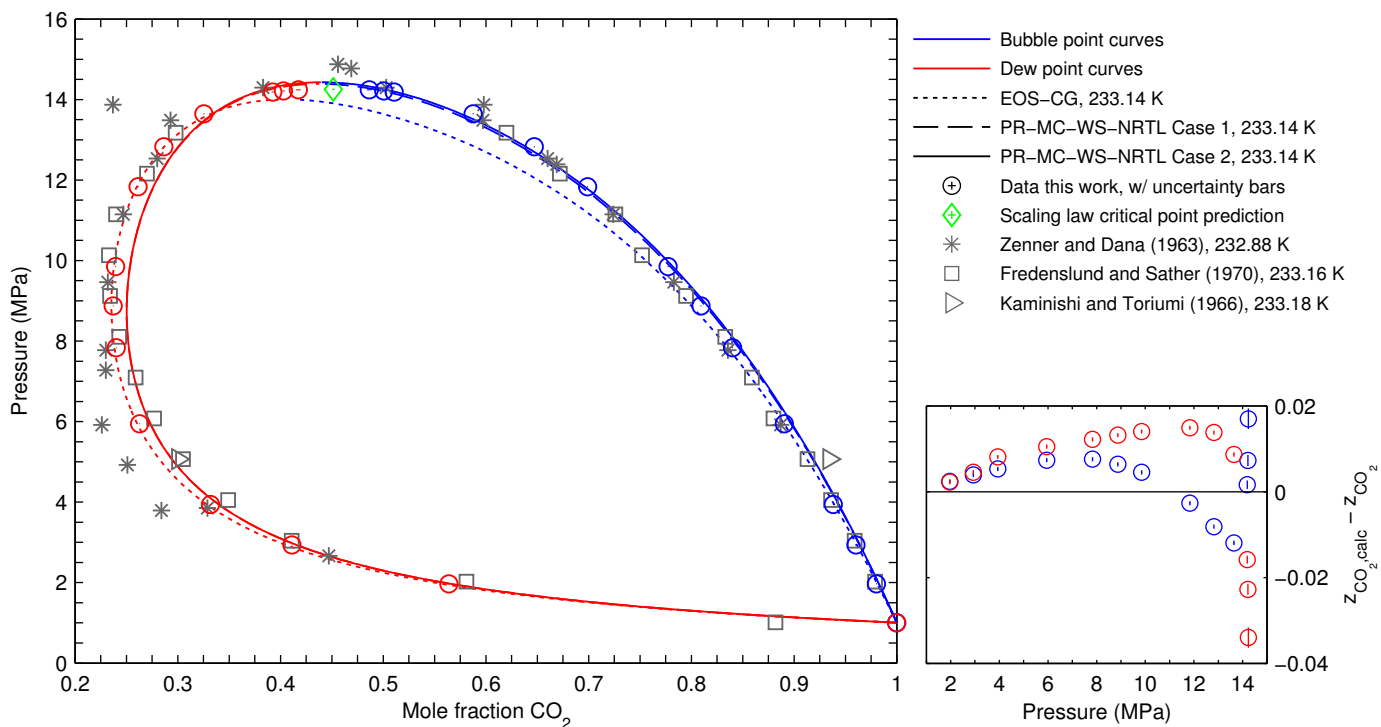
^a Sample standard deviation of the mean of the temperatures $s(\bar{T}_f)$, mean of the standard systematic uncertainty of the temperatures $\bar{u}_c(\bar{T})$, total standard uncertainty of the temperature $u_c(\bar{T}_f)$, sample standard deviation of the mean of the pressures $s(\bar{p}_f)$, mean of the standard systematic uncertainty of the pressures $\bar{u}_c(\bar{p})$, total standard uncertainty of the pressure $u_c(\bar{p}_f)$, sample standard deviation of the mean of the mole fractions $s(\bar{y}_{\text{CO}_2})$, mean of the total standard uncertainty of the mole fractions $\bar{u}_{\text{tot}}(y_{\text{CO}_2})$, final standard uncertainty of the mole fraction $u_c(y_{\text{CO}_2})$, PR-MC-WS-NRTL Case 2 EOS calculated mole fraction $y_{\text{CO}_2,\text{calc}}(\bar{T}_f, \bar{p}_f)$ ^b Span-Wagner CO₂ vapor pressure is 0.5539 ± 0.0002 MPa.

^c Span-Wagner CO₂ vapor pressure is 1.0042 ± 0.0003 MPa. ^d Span-Wagner CO₂ vapor pressure is 1.9694 ± 0.0006 MPa. ^e Span-Wagner CO₂ vapor pressure is 3.4849 ± 0.0010 MPa.

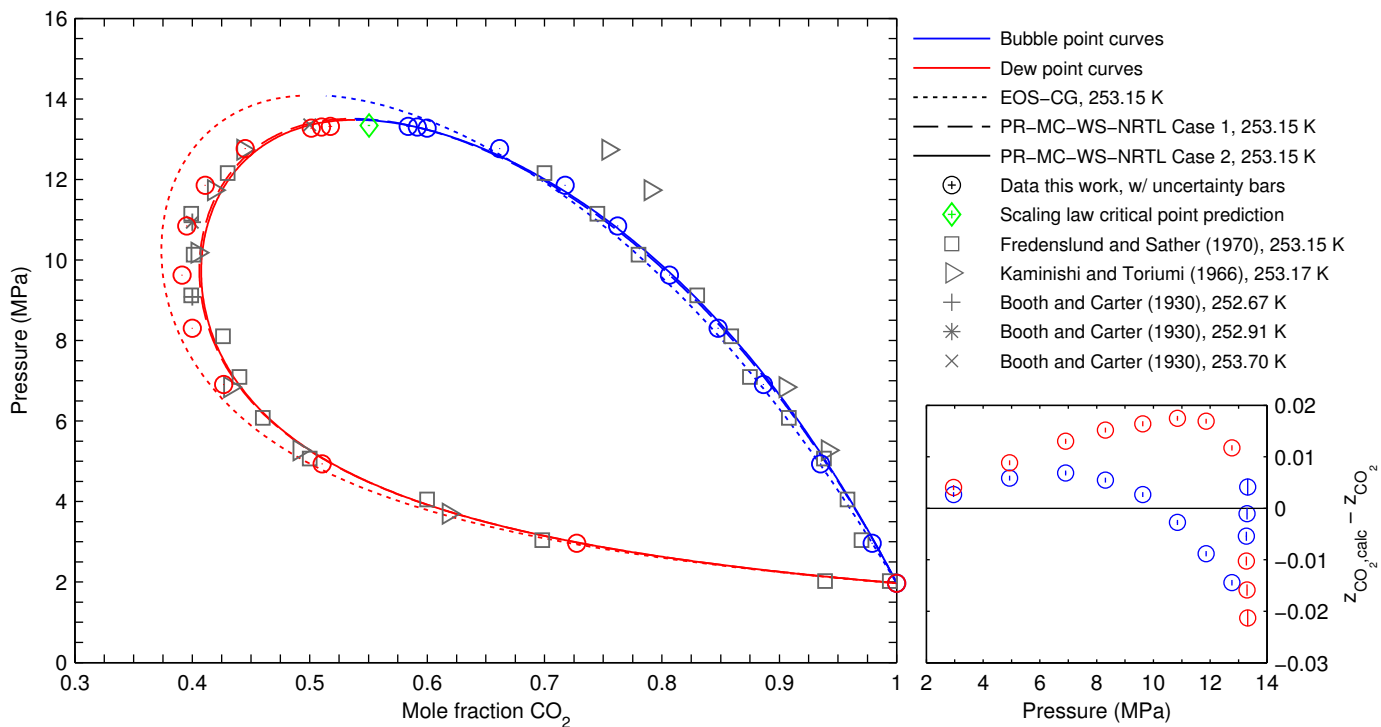
^f Span-Wagner CO₂ vapor pressure is 5.0859 ± 0.0015 MPa. ^g Span-Wagner CO₂ vapor pressure is $6.4324 \pm$



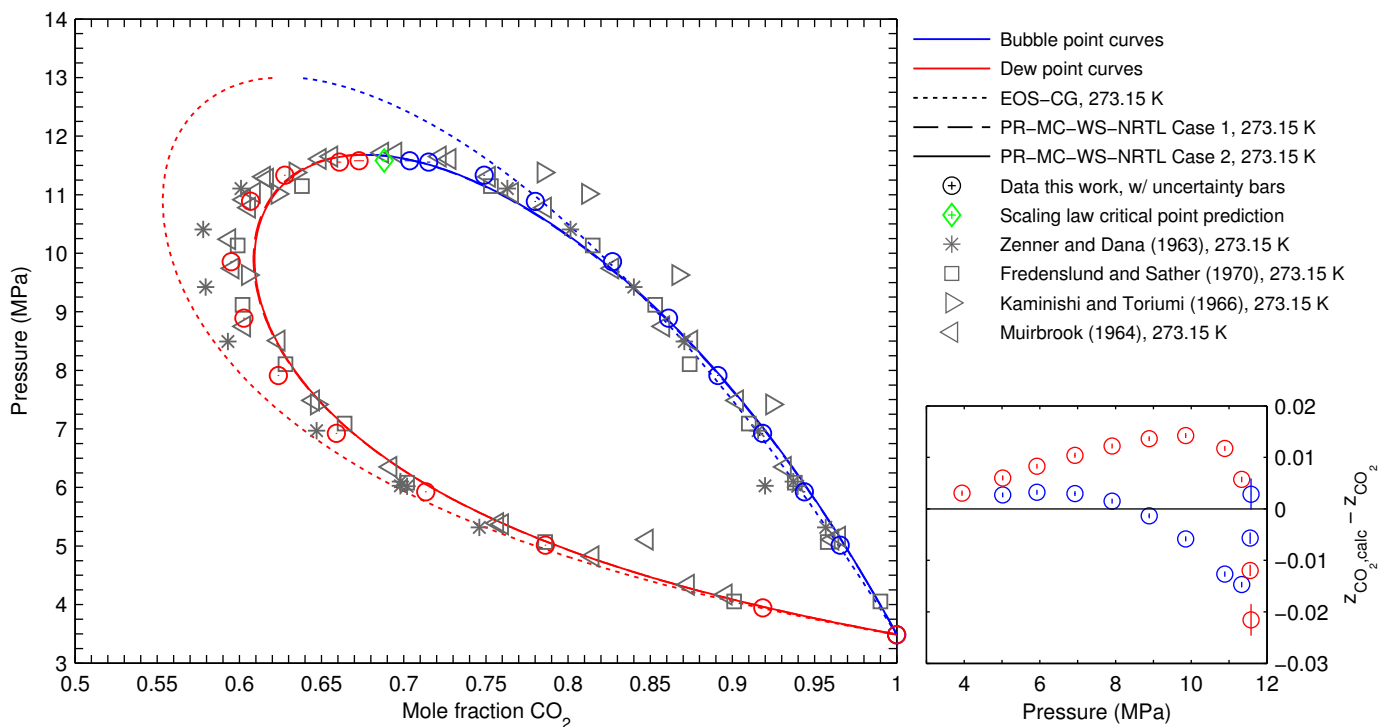
(a) Mean temperature of measurements in present work 218.148 K. VLE data from literature [19].



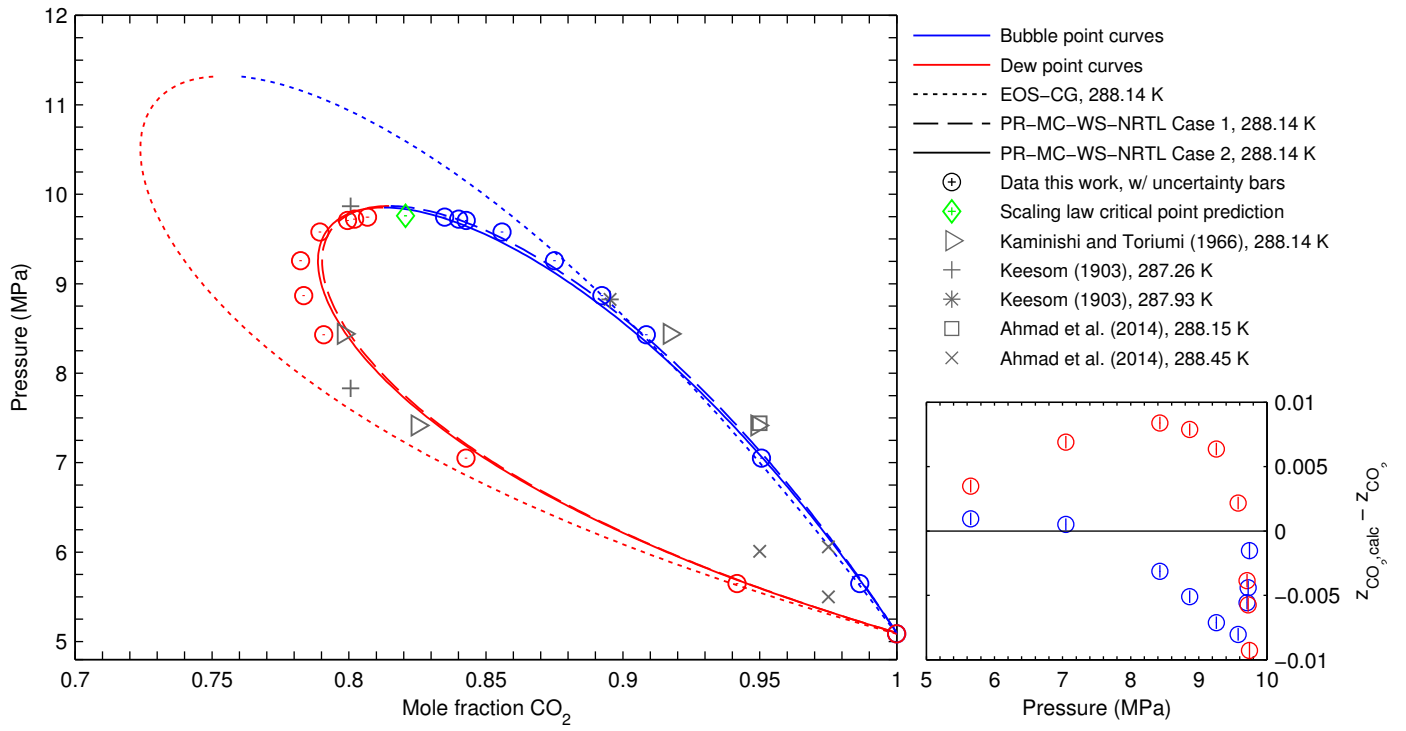
(b) Mean temperature of measurements in present work 233.143 K. VLE data from literature [19, 20, 21].



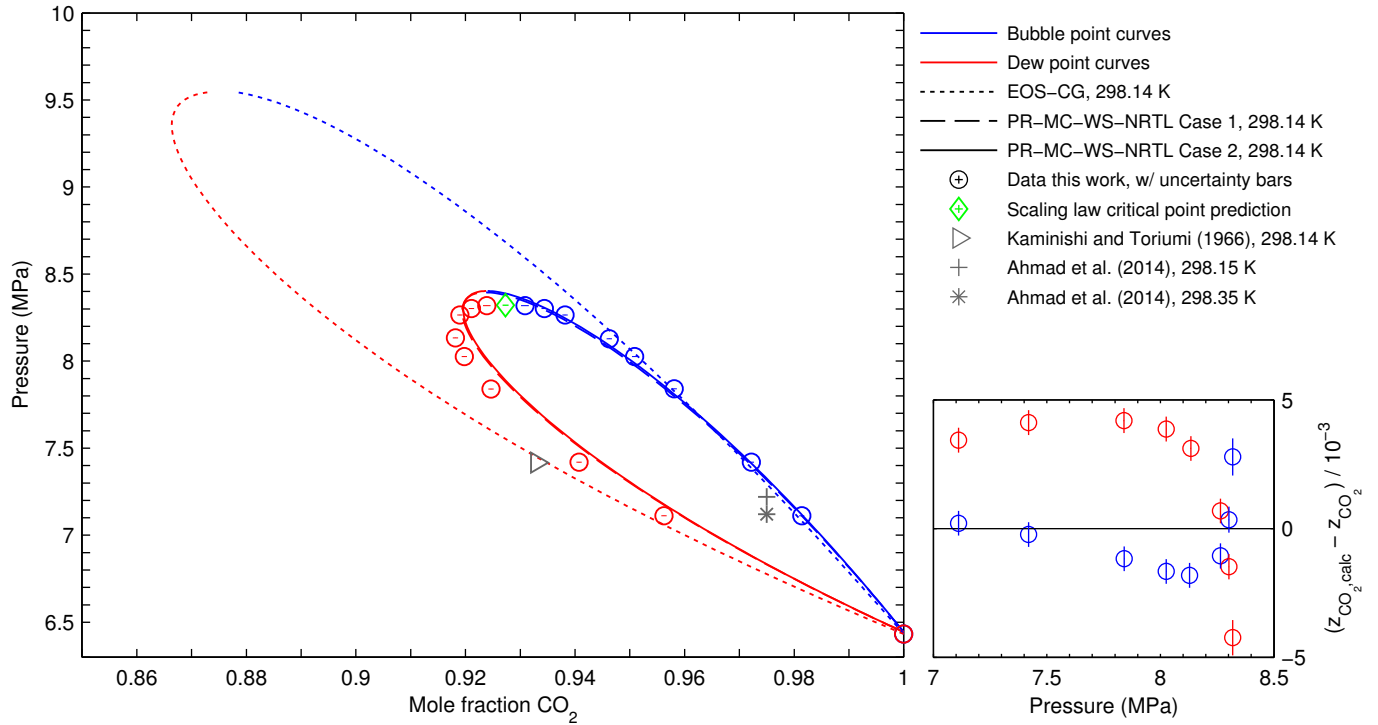
(c) Mean temperature of measurements in present work 253.147 K. VLE data from literature [20, 21, 22].



(d) Mean temperature of measurements in present work 273.146 K. VLE data from literature [19, 20, 21, 23].



(e) Mean temperature of measurements in present work 288.139 K. VLE data from literature [21, 24, 25].



(f) Mean temperature of measurements in present work 298.136 K. VLE data from literature [21, 25].

Fig. 5. Left: Pressure-composition diagram based on EOS calculations at the different mean temperatures, VLE data from literature, and VLE measurements with estimated uncertainties from present work: \bar{x}_{CO_2} , \bar{y}_{CO_2} , \bar{p}_f , $u_c(\bar{x}_{\text{CO}_2})$, $u_c(\bar{y}_{\text{CO}_2})$ and $u_c(\bar{p}_f)$ from Tables 7 and 8. Please note that the uncertainty bars are very small compared to the scale of the plots. Critical point estimation and its uncertainties are from Section 5.3. Right: Plot of deviation between PR-MC-WS-NRTL Case 2 $z_{\text{CO}_2,\text{calc}}$ and VLE measurements from present work z_{CO_2} , where z_{CO_2} is equal to either x_{CO_2} or y_{CO_2} .

Table 9

Composition data at supercritical states for the liquid and vapor samplers for CO₂ (1) + O₂ (2) at mean temperature \bar{T}_f , mean pressure \bar{p}_f , and mean mole fraction \bar{z}_{CO_2} ^a.

| ID | Data | | | Temperature | | | Pressure | | | Composition | |
|-----|--------------------|----------------------|--------------------------------|-----------------------|-----------------------------|-------------------------|-------------------------|-------------------------------|---------------------------|-----------------------------------|-------------------------------------|
| | \bar{T}_f (K) | \bar{p}_f (MPa) | \bar{z}_{CO_2} (-) | $s(\bar{T}_f)$ (K) | $\bar{u}_c(\bar{T})$ (K) | $u_c(\bar{T}_f)$ (K) | $s(\bar{p}_f)$ (MPa) | $\bar{u}_c(\bar{p})$ (MPa) | $u_c(\bar{p}_f)$ (MPa) | $s(\bar{z}_{\text{CO}_2})$ (-) | $u_c(\bar{z}_{\text{CO}_2})$ (-) |
| L12 | 218.148 | 14.4390 | 0.39450 | 2.1e-4 | 3.4e-3 | 3.4e-3 | 1.2e-5 | 2.8e-3 | 2.8e-3 | 4.3e-6 | 4.8e-4 |
| V13 | 218.147 | 14.4390 | 0.39472 | 1.4e-4 | 3.4e-3 | 3.4e-3 | 6.2e-6 | 2.8e-3 | 2.8e-3 | 9.0e-6 | 4.8e-4 |
| L26 | 233.142 | 14.2617 | 0.44465 | 2.5e-4 | 7.4e-3 | 7.4e-3 | 1.3e-5 | 2.8e-3 | 2.8e-3 | 1.1e-5 | 4.8e-4 |
| V27 | 233.142 | 14.2617 | 0.44445 | 7.7e-5 | 7.5e-3 | 7.5e-3 | 1.3e-5 | 2.8e-3 | 2.8e-3 | 9.3e-6 | 4.8e-4 |
| L38 | 253.147 | 13.3560 | 0.55468 | 6.3e-5 | 5.9e-3 | 5.9e-3 | 3.5e-5 | 2.7e-3 | 2.7e-3 | 1.9e-5 | 4.8e-4 |
| V39 | 253.148 | 13.3561 | 0.55470 | 3.3e-5 | 5.6e-3 | 5.6e-3 | 1.3e-4 | 2.7e-3 | 2.7e-3 | 1.3e-5 | 4.8e-4 |
| L49 | 273.146 | 11.5976 | 0.68191 | 4.5e-4 | 2.6e-3 | 2.6e-3 | 9.5e-5 | 2.7e-3 | 2.7e-3 | 1.9e-5 | 4.8e-4 |
| V51 | 273.145 | 11.5975 | 0.68219 | 1.2e-4 | 2.5e-3 | 2.5e-3 | 1.4e-5 | 2.7e-3 | 2.7e-3 | 5.5e-6 | 4.8e-4 |

^a Samples taken using liquid sampler given with ID L, samples taken using vapor sampler given with ID V. Sample standard deviation of the mean of the temperatures $s(\bar{T}_f)$, mean of the standard systematic uncertainty of the temperatures $\bar{u}_c(\bar{T})$, total standard uncertainty of the temperature $u_c(\bar{T}_f)$, sample standard deviation of the mean of the pressures $s(\bar{p}_f)$, mean of the standard systematic uncertainty of the pressures $\bar{u}_c(\bar{p})$, total standard uncertainty of the pressure $u_c(\bar{p}_f)$, sample standard deviation of the mean of the mole fractions $s(\bar{z}_{\text{CO}_2})$. Standard uncertainty in mean of the mole fractions $u_c(\bar{z}_{\text{CO}_2}) = \sqrt{s^2(\bar{z}_{\text{CO}_2}) + \bar{u}^2(\bar{z}_{\text{CO}_2})}$, where $\bar{u}(\bar{z}_{\text{CO}_2})$ is the mean of $u(\bar{z}_{\text{CO}_2})$ for the corresponding series in Table S.4 in the Supplementary Material.

$s(\bar{x}_{\text{CO}_2})$, were $1.3 \cdot 10^{-4}$ and $1.2 \cdot 10^{-5}$, respectively. Similarly, for the vapor phase mole fractions in Table 8, the maximum and average $s(\bar{y}_{\text{CO}_2})$ were respectively $1.2 \cdot 10^{-4}$ and $2.5 \cdot 10^{-5}$. Some of the vapor phase points at the lowest pressures at each temperature showed increase in these standard deviations, as could be expected by the high VLE composition sensitivity to pressure changes. Also, there seemed to be a slight increase in the standard deviations for some of the VLE points at the highest pressures. Inspecting the composition sample data for these points in Tables S.2 and S.3 in the Supplementary Material, the liquid and vapor phase mole fractions were respectively increasing and decreasing slightly throughout the series. This could imply that VLE had not been achieved completely or more likely, that the separation of the phases was incomplete, even though the settling times had been increased significantly for these measurements at close proximity to the critical point, as described in Section 2.3. It can be noted that the observed variations did not exceed the estimated uncertainty of the composition analysis, $4.8 \cdot 10^{-4}$ from Table 6. However, if the cause for the variations was incomplete settling, there is a possibility that the actual VLE compositions are outside the values covered by the composition analysis uncertainty.

The mean standard uncertainty in the phase mole fractions caused by the composition analysis and the temperature and pressure uncertainties described in Section 3.3.5, $\bar{u}_{\text{tot}}(z_{\text{CO}_2})$ where $z_{\text{CO}_2} = x_{\text{CO}_2}$ or y_{CO_2} , increased as a function of pressure at each temperature. At pressures close to the critical points, where the scaling law was used to estimate the VLE composition sensitivity to pressure, $\partial z_{\text{CO}_2} / \partial p$, $\bar{u}_{\text{tot}}(z_{\text{CO}_2})$ was $3.1 \cdot 10^{-3}$ at its maximum. For the series outside the critical region, $\bar{u}_{\text{tot}}(z_{\text{CO}_2})$ was close to the composition analysis uncertainty, $4.8 \cdot 10^{-4}$, as the uncertainties in pressure and temperature did not contribute significantly.

The final standard uncertainty of the mole fractions, $u_c(\bar{z}_{\text{CO}_2})$, combining $s(\bar{z}_{\text{CO}_2})$ and $\bar{u}_{\text{tot}}(z_{\text{CO}_2})$ described above, was maximum $3.1 \cdot 10^{-3}$ for the series in the critical region, and approximately $5 \cdot 10^{-4}$ for the series outside the critical region.

As can be seen in Tables S.2 and S.3 in the Supplemen-

tary Material, the combined standard uncertainty of the measured temperatures, $u_c(\bar{T})$, was below 8 mK for all samples, and around 4 mK on average. The combined standard uncertainty of the measured pressures, $u_c(\bar{p})$, ranged from 0.5 kPa at the lowest measured pressure 0.56 MPa (0.09%) to 3 kPa at the highest measured pressure 14.4 MPa (0.02%).

5.2. Comparison with literature data

The literature data reviews in [2, 3, 4, 5] provided in total five works reporting isothermal analytic VLE measurements [19, 21, 20, 26, 27] and two works reporting synthetic VLE measurements [22, 23]. The work by [27] from 2009 contained isothermal VLE measurements at 240.9 K, and apart from this the other works were from 1972 or earlier. In addition, two works reporting synthetic VLE measurements were found, one from 1903 [24] and the other from 2014 [25]. A summary of these literature data is given in Table 10.

Literature data at temperatures comparable to our measurements [19, 21, 20, 23, 24, 22, 25] are plotted together with our data in Figs. 5a to 5f. These figures give a general overview of the varying agreement between our data and the literature data. However, there are a few aspects of some of the literature data that are not apparent from the figures, which will be discussed here.

The data by Zenner and Dana [19] at 232.88 K were at a slightly lower temperature than our data at 233.14 K, but the data should be comparable as the temperature sensitivity of the VLE compositions are relatively low at these temperatures (cf. Tables S.2 and S.3 in the Supplementary Material). Their data points at approximately 14.85 MPa did not agree with our critical point prediction (See Section 5.3 below). However, Zenner and Dana [19] indicated in their work that these two points were outside the two-phase region.

At 273.15 K, the data by Fredenslund and Sather [20] agreed reasonably well with our data. The authors suggested that their bubble and dew points at 11.2 MPa might be erroneous, caused by entrainment. Our bubble and dew points neighboring these points were at respectively higher

Table 10

Available isothermal (ISOT) and synthetic (SYN) VLE literature data and the temperature, pressure and composition ranges.

| Authors | Year | Type | T (K) | p (MPa) | Composition CO_2 | No. of points |
|-----------------------------|------|------|--|-----------|--------------------------------|-----------------|
| Zenner and Dana [19] | 1963 | ISOT | 218.19, 232.88, 273.15 | 2.2-14.9 | 0.147-0.967 | 58 |
| Kaminishi and Toriumi [21] | 1966 | ISOT | 233.18, 253.17, 273.15, 288.14, 293.14, 298.14 | 3.7-12.7 | 0.300-0.949 | 30 |
| Fredenslund and Sather [20] | 1970 | ISOT | 223.16, 233.16, 243.16, 253.15, 263.15, 273.15, 283.15 | 1.0-13.2 | 0.180-0.994 | 143 |
| Fredenslund et al. [26] | 1972 | ISOT | 223.76 | 0.9-14.2 | 0.186-0.996 | 21 |
| Engberg et al. [27] | 2009 | ISOT | 240.9 | 1.9-7.2 | 0.301-0.986 | 20 |
| Muirbrook [23] | 1964 | ISOT | 273.15 | 4.2-11.7 | 0.594-0.965 | 33 |
| Keesom [24] | 1903 | SYN | 283.21-296.38 | 6.7-10.4 | 0.8006, 0.8953 | 36 |
| Booth and Carter [22] | 1930 | SYN | 212.76-259.91 | 3.6-14.3 | 0.2, 0.3, 0.4, 0.5 | 34 ^a |
| Ahmad et al. [25] | 2014 | SYN | 277.35-298.35 | 4.1-8.1 | 0.9493, 0.9506, 0.9745, 0.9751 | 22 |

^a The authors did not report VLE data directly, only the observed phases present at different pressure-temperature states at constant total composition. VLE data points approximated as mean of state variables where difference in temperature or pressure was small across a liquid to vapor-liquid or vapor to vapor-liquid transition.

and lower CO_2 mole fractions, which indicated that this might be correct.

As can be seen from Figs. 5a to 5f, the agreement between our data and literature data varied significantly, also from one temperature to another by the same author. This highlighted the inconsistencies in the literature data noted in [3, 4, 5]. Compared with the existing literature data, the data in the present work described the VLE at the six measured temperatures with considerably less scatter, and included several measurements in the critical region at each temperature, thus forming a good basis for modeling the system. In addition, the VLE measurements at 288.14 and 298.14 K constituted the only complete isotherms at temperatures above 273.15 K.

5.3. Critical point estimation

The procedure for estimating the critical point in terms of pressure and composition for a binary mixture at a certain temperature utilizing scaling laws from statistical mechanics [28, 29, 30] was described for the use on CO_2+N_2 mixtures in [1]. The same procedure was used for estimating the critical points in the present work, the only exception being the estimation of the uncertainty in the critical composition, which is discussed below. The critical point for a binary mixture in terms of pressure and temperature is dependent on the composition. For a given temperature, the composition, if any, where the critical point is attained, is denoted the critical composition, with symbol $z_{\text{CO}_2,c}$, and the corresponding critical pressure, with symbol p_c , is identified as the point of maximum pressure in closed isothermal pressure-composition phase envelopes for a binary mixture, as seen in Figs. 5a to 5f.

Like in [1], the following scaling law was applied [31, 32]:

$$z_{\text{CO}_2} = \hat{z}_{\text{CO}_2,c} + \left(\lambda_1 - \epsilon \frac{\lambda_2}{2} \right) (\hat{p}_c - p) - \epsilon \frac{\mu}{2} (\hat{p}_c - p)^\beta, \quad (6)$$

where

$$\epsilon = \begin{cases} 1 & \text{for bubble points,} \\ -1 & \text{for dew points,} \end{cases}$$

and z_{CO_2} was the bubble point ($z_{\text{CO}_2} = x_{\text{CO}_2}$) or dew point ($z_{\text{CO}_2} = y_{\text{CO}_2}$) CO_2 mole fraction at pressure p . Keeping β

fixed at 0.325 [33], the critical composition $z_{\text{CO}_2,c}$ and pressure p_c and the parameters λ_1 , λ_2 and μ were fitted at each isotherm average temperature using the VLE data identified in Table 11. The regression was performed using the ordinary unweighted least squares method, giving the estimators $\hat{z}_{\text{CO}_2,c}$, \hat{p}_c , $\hat{\lambda}_1$, $\hat{\lambda}_2$ and $\hat{\mu}$ shown in Table 11.

The uncertainties in the estimated critical composition and pressure, respectively $u(z_{\text{CO}_2,c})$ and $u(\hat{p}_c)$, were estimated according to Eqs. (16) and (17) in [1]. These estimates were based on the uncertainties in the composition and pressure of the VLE data used in the fitting, and the standard errors of regression of the critical composition and pressure, $S_E(\hat{z}_{\text{CO}_2,c})$ and $S_E(\hat{p}_c)$, respectively. The estimates for the uncertainty in the composition of the VLE data used in the fitting, $u_c(\bar{x}_{\text{CO}_2})$ and $u_c(\bar{y}_{\text{CO}_2})$, were calculated based on values for the composition derivatives with respect to pressure, $\partial z_{\text{CO}_2}/\partial p$, derived from Eq. (6). The values that were calculated using the scaling law are given in Tables S.2 and S.3 in the Supplementary Material, and in Tables 7 and 8, indicated with the marker symbol ⁺.

The estimated critical compositions and pressures with their corresponding uncertainties are given in Table 11, and are plotted together with the critical region VLE data and the supercritical state points from Table 9 in Fig. 6.

The standard errors of regression were very low compared to the corresponding uncertainties in the compositions and pressures in the VLE data used for each regression at all temperatures.

Attempts to increase or decrease the number of VLE points used to fit the parameters, compared to the sets of points stated in Table 11, did not result in changes in the critical compositions and pressures that were larger than the uncertainties in these fitted parameters. However, this was only valid if the VLE points closest to the mixture critical points were included in the fit. If fewer of these VLE points were included in the fit, the deviations in the estimated critical compositions and pressures from the estimates given in Table 11 became more pronounced. Two examples are given. First, if the eight VLE points identified as L6-9 and V7-10 in Tables 7 and 8 were used to fit the scaling law at 218.15 K, the estimated critical composition and pressure were respectively 0.4057 and 14.421 MPa. In this data set, the four VLE points closest to the mixture critical point were not included. The estimated critical composition did not change

significantly, considering the uncertainty given in Table 11, $u(\bar{z}_{\text{CO}_2,c}) = 0.00115$. However, the estimated critical pressure decreased with 0.014 MPa. Second, if the data set contained the eight VLE points identified as L5-8 and V6-9 were used for the fit, the estimated critical composition and pressure were respectively 0.4052 and 14.346 MPa. In this data set, the six VLE points closest to the mixture critical point were not included. The estimated critical composition decreased slightly more compared to the estimate given in Table 11. Also, the estimated critical pressure decreased with 0.089 MPa.

The supercritical state point pairs at each temperature in Table 9 showed a small difference in composition. As indicated in Section 2.3.2, there was always a possibility that the content of the cell was in the two-phase region during these measurements, but sufficiently close to the critical point such that critical opalescence (see e.g. Ref. [34]) caused the cell phases to become indiscernible. However, the differences in composition shown in Table 9 were below the estimated uncertainty in the composition analysis, $4.8 \cdot 10^{-4}$. Hence, on this basis, it was not possible to conclude that this difference suggested an actual difference in composition, caused by the presence of two phases. In addition, as Fig. 6 shows, the supercritical state points at 218.15, 233.14, 253.15 and 273.15 K were all at higher pressures than the predicted critical pressures, which supported the assumption that these supercritical measurements were indeed outside the two-phase region.

Based on this discussion, it was assumed that the estimates for the critical points were reasonable, and that the VLE measurements in the critical region also were reasonable, within their corresponding uncertainty estimates and their aforementioned limitations.

5.4. Model fitting

5.4.1. Introduction

In [1], the model for the CO_2+N_2 system in the equation of state called EOS-CG [3, 4] was fitted to the VLE data measured in [1]. The highly flexible structure of the GERG-2008 EOS [35], developed for natural gas mixtures, was used by Gernert and Span [3] to develop EOS-CG, which was fitted to data for the mixtures of some of the components expected in captured CO_2 in CCS processes [3]. The model and parameters used for the CO_2+N_2 system in EOS-CG were almost unchanged compared to that used in the GERG-2008 [3]. The EOS-CG model for the CO_2+O_2 system was an improvement compared to that of the GERG-2008 model. However, as noted in [3, 4], some restrictions on the number of fitting parameters and number of terms utilized in EOS-CG were set due to the inferior data situation. The quality of the description of the CO_2+O_2 system by EOS-CG was reduced accordingly.

The EOS-CG model calculations are plotted in Figs. 5a to 5f. The deviations between the model and the new data of this work were significant. The VLE data provided in the present work considerably improved the data situation for

the CO_2+O_2 system, and can be used together with the other available literature data for VLE and properties such as density and speed of sound, to improve the model description of the system.

In this work, the parameters of the Peng-Robinson (PR) cubic EOS [36] with the alpha correction by Mathias and Copeman [37] (MC), the mixing rules by Wong and Sandler [38] (WS), and the NRTL [39] excess Gibbs energy model were fitted. This combination of EOS, alpha correction, mixing rule, and excess Gibbs energy model, designated here as PR-MC-WS-NRTL, has been used with some success to fit VLE data of binary systems containing one supercritical component in our previous work [1] (CO_2+N_2) and in the work of Coquelet et al. [40] (CO_2+Ar).

The data in Tables 7 and 8 formed the basis for the model fitting. Similar to [1], the fitting was performed using orthogonal distance regression (ODR) [41]. ODR is particularly suited to fit data where both the dependent and independent data have significant uncertainty. In this work, the distances between the VLE data points (\bar{z}_{i,CO_2} , $\bar{p}_{i,f}$) for each temperature and the corresponding closest point of the model prediction ($z_{i,\text{CO}_2,\text{calc}}$, $p_{i,\text{calc}}$) were calculated, where the deviations in composition and pressure were normalized with their respective uncertainties. \bar{z}_{CO_2} is equal to either \bar{x}_{CO_2} or \bar{y}_{CO_2} . The objective function can be stated as

$$S^2 = \frac{1}{n - n_p} \sum_i \left(\frac{p_{i,\text{calc}} - \bar{p}_{i,f}}{u_c(\bar{p}_{i,f})} \right)^2 + \frac{1}{n - n_p} \sum_i \left(\frac{z_{i,\text{CO}_2,\text{calc}} - \bar{z}_{i,\text{CO}_2}}{u(z_{\text{CO}_2})} \right)^2, \quad (7)$$

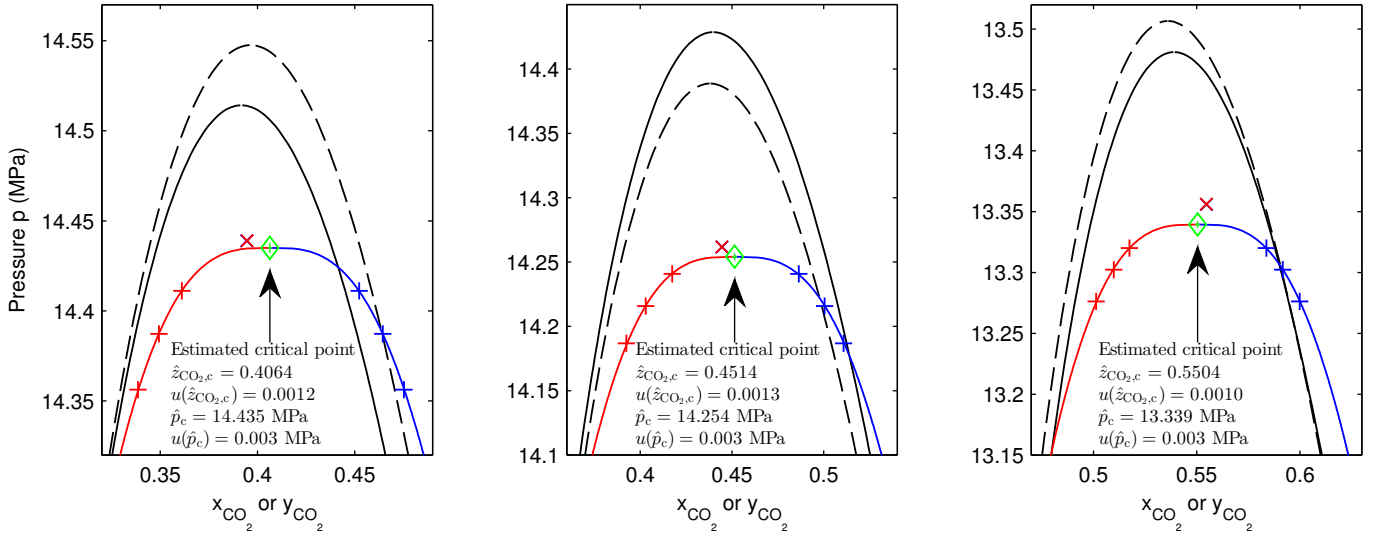
where n is the total number of experimental data points, n_p is the number of parameters adjusted in the model fit and $u(z_{\text{CO}_2})$ is the composition uncertainty caused by the analysis given in Table 6. In addition to S , two other statistics were used to quantify the agreement between model and data: the absolute average deviation (AAD) and the bias (BIAS), whose formulas are given in Table 12.

5.4.2. Peng-Robinson EOS

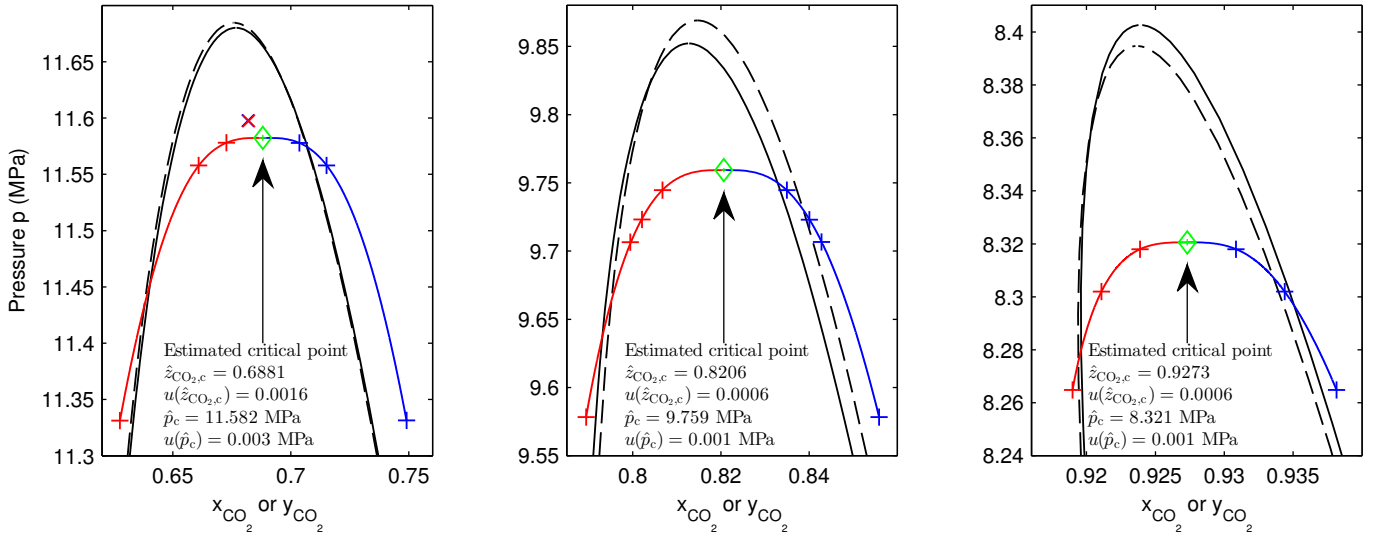
The formulas and corresponding nomenclature used in the present work for the MC alpha correction [37], the WS mixing rules [38] and the NRTL [39] excess Gibbs energy model were given in [1] and are not reproduced here. The critical temperature and pressure used in the EOS phase equilibrium calculations for $i = \text{CO}_2$ or O_2 are given in Table 13, together with the parameters $c_{1,i}$, $c_{2,i}$ and $c_{3,i}$ used in the MC alpha correction.

The parameters of the PR-MC-WS-NRTL EOS consist of the Wong-Sandler binary interaction parameters, k_{ij} , the binary interaction parameters of the NRTL model, τ_{ij} , and the non-randomness parameters of the NRTL model, α_{ij} .

These parameters were restricted according to Eq. (27) in [1], and a constant value for $\alpha_{12} = \alpha_{21} = 0.3$ was assumed for a system of two non-polar components such as CO_2+O_2



(a) 218.15 K. The figure shows only 6 of the 8 VLE points used for fitting the scaling law. (b) 233.14 K. The figure shows only 6 of the 8 VLE points used for fitting the scaling law. (c) 253.15 K. The figure shows only 6 of the 8 VLE points used for fitting the scaling law.



(d) 273.15 K. (e) 288.14 K. (f) 298.14 K.

- + Liquid phase measurements used for fitting scaling law
- + Vapor phase measurements used for fitting scaling law
- × Supercritical measurements taken using liquid phase sampler
- × Supercritical measurements taken using vapor phase sampler

- Scaling law bubble point curve
- Scaling law dew point curve
- PR-MC-WS-NRTL Case 1
- PR-MC-WS-NRTL Case 2

Fig. 6. Comparison of the predictions of the pressure-composition phase behavior in the critical region by three different models: PR-MC-WS-NRTL Case 1 and Case 2 EOSs, and the scaling law model in Eq. (6). Please note that the scales of the graphs are very different from each other. Please refer to Table 11 for an overview of the VLE points used to fit the scaling law and the parameters at the different temperatures. Supercritical measurements are shown in Table 9.

Table 11

Parameters of the scaling law in Eq. (6) fitted to critical region data from this work at six different average temperatures.

| T (K) | Used points ^a | n_p (-) | $\tilde{\lambda}_1$ (MPa ⁻¹) | $\tilde{\lambda}_2$ (MPa ⁻¹) | $\tilde{\mu}$ (MPa ^{-β)} | $\tilde{z}_{\text{CO}_2,c}$ (-) | \tilde{p}_c (MPa) | $S_E(\tilde{z}_{\text{CO}_2,c})$ (-) | $u(\tilde{z}_{\text{CO}_2,c})$ (-) | $S_E(\tilde{p}_c)$ (MPa) | $u(\tilde{p}_c)$ (MPa) |
|------------|--------------------------|--------------|---|---|---|------------------------------------|------------------------|---|---------------------------------------|-----------------------------|---------------------------|
| 218.148 | L8-11, V9-12 | 8 | $8.8655 \cdot 10^{-3}$ | $-5.6184 \cdot 10^{-2}$ | -0.30221 | 0.4064 | 14.435 | $7.3 \cdot 10^{-5}$ | 0.00115 | $3.6 \cdot 10^{-4}$ | 0.0028 |
| 233.143 | L22-25, V23-26 | 8 | $8.3022 \cdot 10^{-3}$ | $-4.3134 \cdot 10^{-2}$ | -0.27699 | 0.4514 | 14.254 | $2.1 \cdot 10^{-4}$ | 0.00130 | $6.3 \cdot 10^{-4}$ | 0.0028 |
| 253.147 | L34-37, V35-38 | 8 | $5.0483 \cdot 10^{-3}$ | $-3.5444 \cdot 10^{-2}$ | -0.23569 | 0.5504 | 13.339 | $1.1 \cdot 10^{-4}$ | 0.00104 | $6.3 \cdot 10^{-4}$ | 0.0028 |
| 273.146 | L46-48, V48-50 | 6 | $8.5843 \cdot 10^{-4}$ | $-3.0614 \cdot 10^{-2}$ | -0.17810 | 0.6881 | 11.582 | $7.0 \cdot 10^{-5}$ | 0.00156 | $1.3 \cdot 10^{-4}$ | 0.0027 |
| 288.139 | L55-58, V57-60 | 8 | $1.1095 \cdot 10^{-2}$ | $-1.8503 \cdot 10^{-2}$ | -0.11004 | 0.8206 | 9.759 | $5.7 \cdot 10^{-5}$ | 0.00055 | $5.1 \cdot 10^{-4}$ | 0.0015 |
| 298.136 | L64-66, V66-68 | 6 | $2.2534 \cdot 10^{-2}$ | $-5.7951 \cdot 10^{-3}$ | -0.048162 | 0.9273 | 8.321 | $5.6 \cdot 10^{-6}$ | 0.00056 | $2.5 \cdot 10^{-5}$ | 0.0012 |

^a Data from Tables 7 and 8, identified with the given IDs.

[39] (cf. [1, 40]). This leaves $n_p = 3$ adjustable parameters in the PR-MC-WS-NRTL model: k_{12} , τ_{12} and τ_{21} . These parameters were assumed to be temperature dependent, to obtain the best possible fit of the data. It was therefore of interest to fit the parameters to data at different temperatures, and try to determine a model for the temperature dependence of the parameters, enabling the use of the EOS over the whole temperature range of the data.

The parameters of the model were fitted to the data at each of the average temperatures 218.15, 233.14, 253.15, 273.15, 288.14 and 298.14 K. The fitted parameters for each temperature are given in Table 12 and plotted in Figs. 7a and 7b, denoted as Case 1. For the temperatures where there were several measurements close to the critical point, only the measurements at the highest pressure were included in the fit, in order to avoid a too strong emphasis on this region. An overview of the points that were excluded are given in Table 12.

With reference to Fig. 7a, the temperature dependencies of τ_{12} and τ_{21} could be approximately described by the function given in [42]:

$$\tau_{12}(T) = a_{\tau_{12}} + b_{\tau_{12}} \cdot \left| (T - T_{c,\text{CO}_2}) / T_{c,\text{CO}_2} \right|^{c_{\tau_{12}}}, \quad (8)$$

$$\tau_{21}(T) = a_{\tau_{21}} + b_{\tau_{21}} \cdot \left| (T - T_{c,\text{CO}_2}) / T_{c,\text{CO}_2} \right|^{c_{\tau_{21}}}. \quad (9)$$

Similarly, with reference to Fig. 7b, the temperature dependency of k_{12} was assumed to be described by a simple linear relationship:

$$k_{12}(T) = a_{k_{12}} + b_{k_{12}} \cdot (T - T_{c,\text{CO}_2}) / T_{c,\text{CO}_2}. \quad (10)$$

With T_{c,CO_2} given in Table 13, the parameters $a_{\tau_{ij}}$, $b_{\tau_{ij}}$, $c_{\tau_{ij}}$, $a_{k_{12}}$ and $b_{k_{12}}$ in Eqs. (8), (9) and (10) were fitted using ordinary unweighted least squares to the optimal Case 1 parameters in Table 12. The fitted parameters of these equations and the calculated values of τ_{12} , τ_{21} , and k_{12} are given in the same table, denoted as Case 2. These calculated Case 2 EOS parameters are plotted in Figs. 7a and 7b with the optimal Case 1 parameters.

The VLE predictions of the PR-MC-WS-NRTL model using both the Case 1 and 2 parameters are shown in Figs. 5a to 5f together with the data from this work and literature. In addition, the deviations between the Case 2 calculated mole fractions and the experimental values are plotted in these

figures. The objective function value, absolute average deviation and bias for both cases are given in Table 12.

With reference to Figs. 5a to 5f, the description of our measurements by the Case 2 model was very close to that of the Case 1 model, and this was reflected with only a minor increase in the values for S and AAD, as seen in Table 12. Therefore, for simplicity, only the Case 2 model will now be discussed. First, the model will be compared with our data, and, second, with the literature data in Table 10.

With reference to our measurement data, three aspects of the Case 2 model could be observed. First, except in the critical region, the vapor CO_2 compositions were slightly overestimated by the model, as seen in Figs. 5a to 5f. In fact, the deviations in composition were in general the largest for the vapor phase, as seen from the pressure-composition deviation plots in these figures. With reference to Table 12, the largest absolute average deviation (AAD), including both liquid and vapor measurements, was 0.01 in mole fraction, which was approximately 3 times larger than the maximum final standard uncertainty of the mole fractions, $u_c(\tilde{z}_{\text{CO}_2})$, $3.1 \cdot 10^{-3}$. Second, the match between the Case 2 model critical points and those estimated by the scaling law in Section 5.3, was quite good, as seen in Figs. 6a to 6f. The critical pressures estimated by the PR-MC-WS-NRTL Case 2 model were approximately 1% higher than the pressures predicted by the scaling law, and the differences in critical compositions were less than 0.015. Third, as seen in the pressure-composition deviation plots in Figs. 5a to 5f, for each of the isotherms the deviation in composition seemed to develop in a similar manner as a function of pressure, with no apparent scatter. If there had been any apparent scatter, there would have been reason to suspect that the composition samples of the series that deviated from the pattern did not represent the composition at VLE. To be precise, the absence of scatter indicated that the samples represented the VLE composition, however not necessarily that the measured mole fractions for these samples were correct.

As the PR-MC-WS-NRTL Case 2 model was fitted against our data only, it was of interest to compare the model with the literature data in Table 10, and especially the data at other temperatures than those we measured. Table 14 shows the AAD and BIAS for the different VLE literature data in Table 10. Since the AAD and BIAS were calculated as the difference between experimental and calculated mole fractions, the values will in general be higher if a data set contained

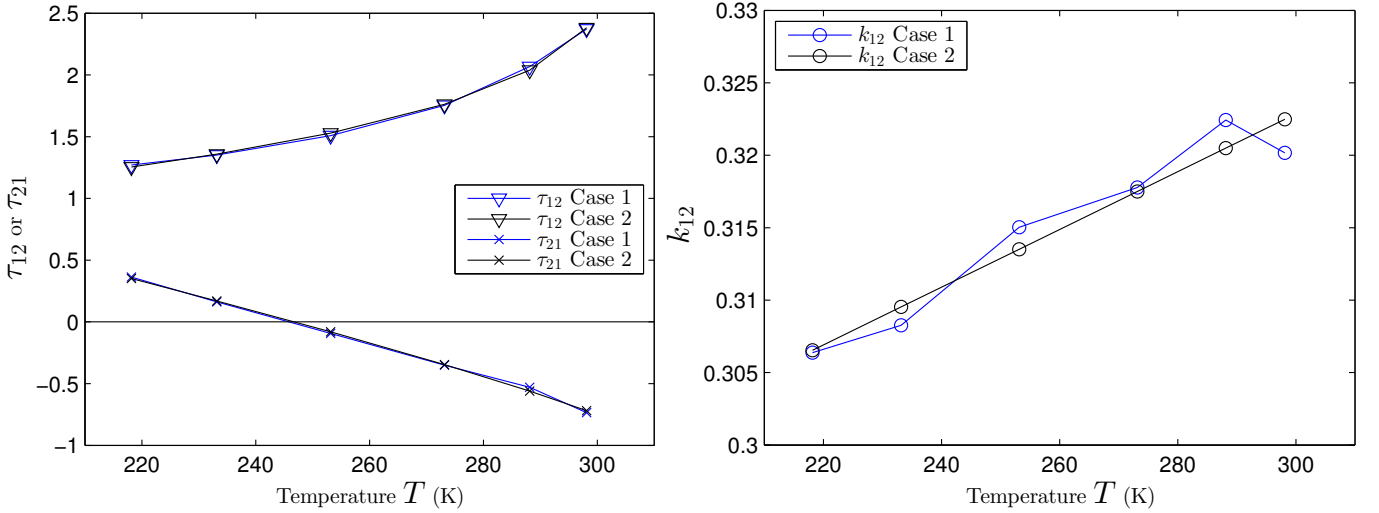
Table 12

Optimal parameters k_{12} , τ_{12} and τ_{21} for the PR-MC-WS-NRTL model, fitted against data from the present work. Objective function S^c and absolute average deviation AAD^d and bias BIAS^e.

| T (K) | Case 1 ^a | | | | | | Case 2 ^b | | | | | | Both cases |
|---------|---------------------|-------------|-------------|-------|---------|----------|---------------------|-------------|-------------|-------|---------|----------|-----------------|
| | k_{12} | τ_{12} | τ_{21} | S | AAD (%) | BIAS (%) | k_{12} | τ_{12} | τ_{21} | S | AAD (%) | BIAS (%) | Excluded points |
| 218.148 | 0.306378 | 1.271116 | 0.362629 | 16.98 | 0.74 | -0.26 | 0.3065 | 1.2536 | 0.3510 | 18.75 | 0.77 | -0.02 | L9-10, V10-11 |
| 233.143 | 0.308267 | 1.351550 | 0.161755 | 22.38 | 0.94 | -0.34 | 0.3095 | 1.3578 | 0.1698 | 23.02 | 0.97 | -0.45 | L23-24, V24-25 |
| 253.147 | 0.315030 | 1.507658 | -0.093799 | 24.48 | 0.96 | -0.30 | 0.3135 | 1.5281 | -0.0806 | 24.91 | 0.99 | -0.47 | L35-36, V36-37 |
| 273.146 | 0.317778 | 1.753552 | -0.350178 | 20.70 | 0.80 | -0.17 | 0.3175 | 1.7628 | -0.3453 | 20.74 | 0.81 | -0.22 | L47, V49 |
| 288.139 | 0.322426 | 2.067354 | -0.529082 | 11.90 | 0.44 | -0.09 | 0.3205 | 2.0384 | -0.5598 | 12.81 | 0.50 | 0.10 | |
| 298.136 | 0.320166 | 2.370883 | -0.735367 | 5.89 | 0.22 | -0.03 | 0.3225 | 2.3813 | -0.7190 | 5.97 | 0.21 | -0.07 | |

^a $k_{12} = k_{21}$ varies freely, $\alpha = 0.3$ ^b $\alpha = 0.3$. τ_{12} , τ_{21} and $k_{12} = k_{21}$ calculated from Eqs. (8), (9) and (10) respectively using $a_{\tau_{12}} = 3.87841$, $b_{\tau_{12}} = -3.42853$, $c_{\tau_{12}} = 0.211545$, $a_{\tau_{21}} = -0.839864$, $b_{\tau_{21}} = 3.53709$, $c_{\tau_{21}} = 0.862063$, $a_{k_{12}} = 0.323688$, $b_{k_{12}} = 0.0606321$ and $T_{c,CO_2} = 304.19$ K from Table 13. ^c Number of parameters fitted $n_p = 3$.

^d $AAD = (100/n) \sum_i |z_{i,CO_2} - z_{i,CO_2,calc}|$ ^e $BIAS = (100/n) \sum_i (z_{i,CO_2} - z_{i,CO_2,calc})$



(a) Optimal values for τ_{12} and τ_{21} for the different temperature data sets in Table 12. (b) Optimal values for k_{12} for the different temperature data sets in Table 12.

Fig. 7. Optimal values for τ_{12} , τ_{21} and k_{12} for the different temperature data sets in Table 12.

data in the critical region. The data sets that contained critical region data with proximity to the critical point comparable to our data are identified in Table 14. The AAD for these data sets were comparable to or higher than the AAD for our data at similar temperatures. The same was valid for the literature data sets in general, with a maximum AAD of 0.025 in mole fraction.

The synthetic VLE data sets in Tables 10 and 14 are plotted in a pressure-temperature phase diagram in Fig. 8, together with the PR-MC-WS-NRTL Case 2 VLE calculations at constant compositions. As seen from this figure, the data by Booth and Carter [22] and Ahmad et al. [25] deviated more from the model than the data by Keesom [24].

As it was not possible to find any literature data at temperatures above 298 K (see Table 10), it was difficult to determine how well the PR-MC-WS-NRTL Case 2 model extrapolates up to the critical temperature of CO₂ at 304.19 K.

It has been established that the PR-MC-WS-NRTL Case 2 model provides a fairly accurate description of the VLE for the CO₂+O₂ system given by our data from the temperatures 218 to 298 K, with an AAD of maximum 0.01 in mole fraction and an apparently good description of the critical locus. The most significant shortcoming of the model was the description of the vapor phase compositions, where the deviations were at their largest. With respect to the ability of the model to describe the literature data, the AAD were comparable or somewhat higher considering the lack of critical region data for most of the literature data sets.

6. Conclusions

This work reports accurate vapor-liquid equilibrium (VLE) data for the CO₂+O₂ binary system, at the temperatures 218.15, 233.14, 253.15, 273.15, 288.14 and 298.14 K.

The data measured in this study cover a large range of VLE liquid and vapor phase compositions, spanning CO₂ mole fractions from approximately 0.45 to 0.987 in the liquid phase, and from 0.15 to 0.956 in the vapor phase. The measured CO₂ vapor pressures at the six temperatures are consistent with the values calculated from the Span-Wagner EOS, considering the uncertainty in both the measured pressures and that of the EOS. The agreement between our data and literature data varies significantly, also from one temperature to another by the same author. This highlights the inconsistencies in the literature data noted in [3, 4, 5]. As in [1], it was possible to perform very stable measurements close to the mixture critical point at each temperature, and these

Table 13

Critical properties^a and Mathias-Copeman coefficients^b used in PR-MC-WS-NRTL EOS for CO₂ and O₂.

| <i>i</i> | $T_{c,i}$ (K) | $p_{c,i}$ (MPa) | $c_{1,i}$ | $c_{2,i}$ | $c_{3,i}$ |
|-----------------|---------------|-----------------|-----------|-----------|-----------|
| CO ₂ | 304.19 | 7.381 | 0.7050 | -0.3185 | 1.9012 |
| O ₂ | 154.58 | 5.043 | 0.4133 | -0.0190 | 0.0944 |

^a From Chiavone-Filho et al. [43]. Slightly different from the values used in [6] and [44]: $T_{c,CO_2} = 304.1282$ K, $p_{c,CO_2} = 7.3773$ MPa, $T_{c,O_2} = 154.581$ K, $p_{c,O_2} = 5.043$ MPa. ^b From Chiavone-Filho et al. [43].

Table 14

AAD and BIAS for the literature data in Table 10, calculated^a using the PR-MC-WS-NRTL Case 2 model.

| Authors | Type | $T^b, z_{CO_2}^c$ (K), (-) | AAD (%) | BIAS (%) | n^d |
|-----------------------------|------|-------------------------------|------------|-------------|-----------------|
| Zenner and Dana [19] | ISOT | 218.19 | 1.29 | -0.76 | 16 |
| | | 232.88 | 2.36 | -1.70 | 22 ^g |
| | | 273.15 | 1.49 | -1.29 | 18 |
| Kaminishi and Toriumi [21] | ISOT | 233.18 | 1.02 | 1.02 | 2 |
| | | 253.17 | 2.46 | 1.46 | 10 |
| | | 273.15 | 2.16 | 1.89 | 8 |
| | | 288.14 | 0.73 | 0.31 | 4 |
| | | 293.14 | 0.82 | 0.13 | 5 |
| Fredenslund and Sather [20] | ISOT | 298.14 | 1.19 | -1.19 | 1 |
| | | 223.16 | 0.83 | -0.79 | 26 |
| | | 233.16 | 1.50 | -0.93 | 25 |
| | | 243.16 | 1.06 | -0.99 | 22 |
| | | 253.15 | 0.92 | -0.57 | 22 |
| | | 263.15 | 0.65 | -0.13 | 20 |
| | | 273.15 | 0.63 | -0.30 | 16 |
| Fredenslund et al. [26] | ISOT | 283.15 | 1.27 | -0.76 | 12 |
| | | 223.76 | 1.79 | 1.24 | 21 ^g |
| Engberg et al. [27] | ISOT | 240.9 | 1.08 | -1.08 | 20 |
| Muirbrook [23] | ISOT | 273.15 | 1.10 | 0.06 | 31 ^g |
| Keesom [24] | SYN | 0.8006 | 2.00 | -1.77 | 10 ^g |
| | | 0.8953 | 0.74 | -0.40 | 26 ^g |
| Booth and Carter [22] | SYN | 0.2 | 1.67 | -1.31 | 9 |
| | | 0.3 | 1.27 | -0.73 | 8 |
| | | 0.4 | 1.56 | -1.05 | 11 ^g |
| | | 0.5 | 2.04 | 1.20 | 6 ^g |
| Ahmad et al. [25] | SYN | 0.9493 ^e | 2.38 | 2.38 | 5 ^g |
| | | 0.9506 ^f | 0.90 | 0.90 | 5 ^g |
| | | 0.9745 ^e | 1.01 | 1.01 | 6 ^g |
| | | 0.9751 ^f | 0.22 | -0.20 | 6 ^g |

^a CO₂ mole fractions at VLE calculated at the temperature and pressure given in the literature data. ^b Temperature T if type is ISOT. ^c z_{CO_2} CO₂ mole fraction if type is SYN. ^d Number of temperature and pressure points that were in the VLE region according to the PR-MC-WS-NRTL Case 2 model. ^e Dew points. ^f Bubble points. ^g Data set contains critical region data.

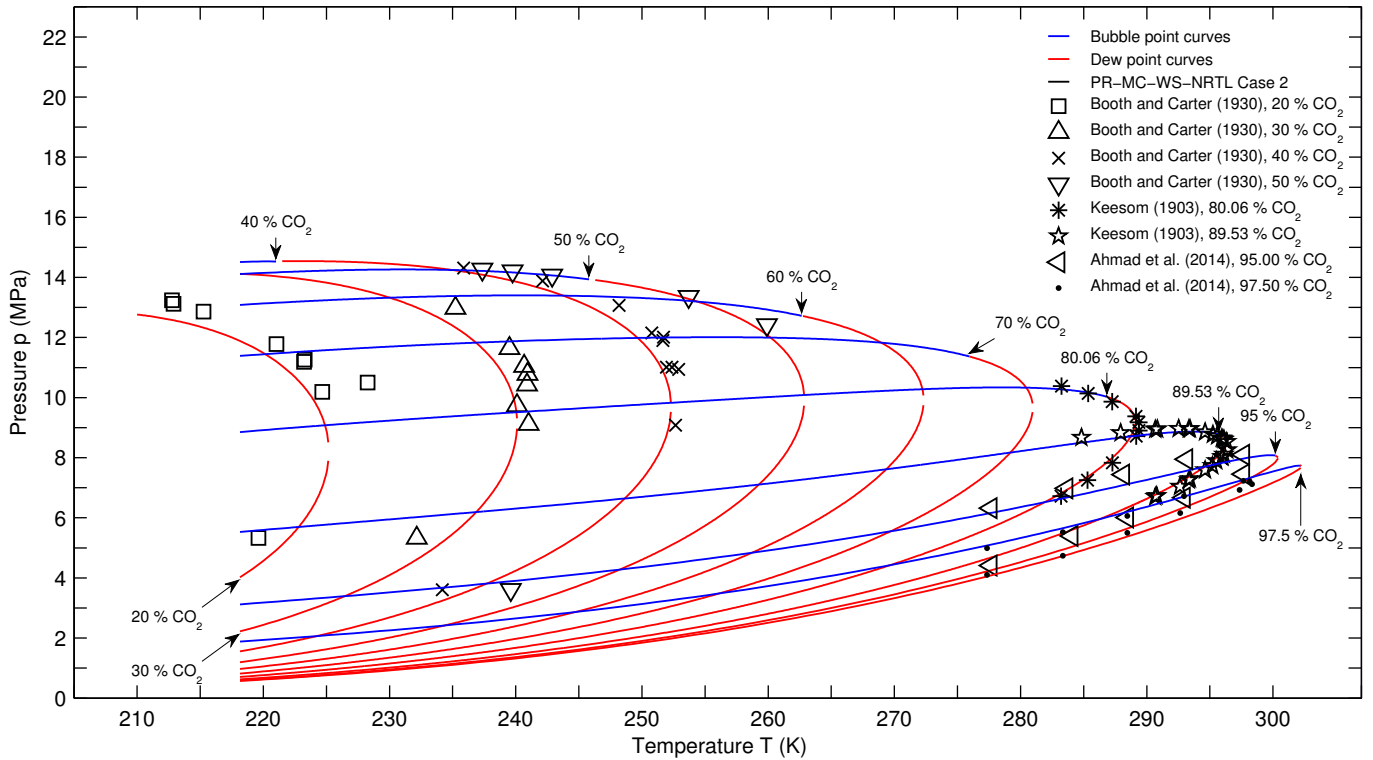


Fig. 8. Pressure-temperature phase diagram at constant compositions based on the PR-MC-WS-NRTL Case 2 model, and synthetic VLE data from literature [22, 24, 25].

data formed the basis for the fitting of a scaling law, resulting in estimates for the critical points with low uncertainties. These critical point estimates were slightly lower in pressure than supercritical state point measurements performed at each temperature, which showed the consistency of the critical point estimates.

The Peng-Robinson (PR) cubic EOS [36] with the alpha correction by Mathias and Copeman [37] (MC), the mixing rules by Wong and Sandler [38] (WS), and the NRTL [39] excess Gibbs energy model was fitted to the data in the present work. Based on the parameters sets at each of the six temperatures, expressions for the temperature dependencies of the parameters were developed, resulting in an EOS that can be utilized for VLE calculations over the temperature range from 218 to 298 K and possibly be extrapolated to the critical temperature of CO₂ at 304.19 K. This model described our data quite accurately, and absolute average deviation of our data compared to this model was maximum 0.01 in mole fraction, and maximum 0.025 for the literature data. Additionally, the model matched well with the critical locus given by the scaling law predictions. The critical points calculated by the PR-MC-WS-NRTL model differed from the scaling law prediction by being approximately 1% higher in pressure, and differed in critical compositions with less than 0.015.

The data measured in the present work showed significantly less scatter than the data found in literature, and included measurements close to the mixture critical points for

all six temperatures. This data set significantly improves the data situation for the CO₂+O₂ system. It can be used to enhance highly flexible multi-parameter equations of state such as EOS-CG [3, 4], which should be able to describe other thermodynamic properties of the system more accurately than the PR-MC-WS-NRTL model fit provided in the present work.

Acknowledgements

This publication has been produced with support from the research program CLIMIT and the BIGCCS Centre, performed under the Norwegian research program Centres for Environment-friendly Energy Research (FME). The authors acknowledge the following partners for their contributions: Gassco, Shell, Statoil, TOTAL, ENGIE and the Research Council of Norway (193816/S60 and 200005/S60).

The research leading to these results has also received funding from the European Community's Seventh Framework Programme (FP7-ENERGY-20121-1-2STAGE) under grant agreement n° 308809 (The IMPACTS project). The authors acknowledge the project partners and the following funding partners for their contributions: Statoil Petroleum AS, Lundin Norway AS, Gas Natural Fenosa, MAN Diesel & Turbo SE and Vattenfall AB.

The authors would like to thank Dr. Morten Hammer, Dr. Geir Skaugen, Dr. Øivind Wilhelmsen, Eskil Aursand and

Magnus Aashammer Gjennestad at SINTEF Energy Research for the in-house software used for VLE calculations and the model fitting. We would also like to thank Håvard Rekstad and Reidar Tellebon of NTNU, and Ingeborg Treu Røe who was a summer intern at SINTEF Energy Research, for their contributions.

Finally, the authors would like to thank Professor Roland Span of Ruhr-Universität Bochum and Dr. Johannes Gernert for the access to their literature data base [3].

τ_{ij} NRTL parameter for binary interaction between components i and j in Eq. (26) in [1]. (–)

Subscripts

c critical state

Superscripts

– arithmetic mean

Abbreviations

AAD absolute average deviation. See Section 5.4.1 and Table 12.

BIAS bias. See Section 5.4.1 and Table 12.

CAD computer-aided design

CCS carbon capture, transport and storage

EOS equation of state

EOS-CG equation of state for combustion gases and combustion gas like mixtures [3, 4]

GC gas chromatograph

GUM ISO Guide for the Estimation of Uncertainty in Measurement [12]

ITS-90 International Temperature Scale of 1990 [45]

MC Mathias-Copeman alpha correction [37]

NRTL non-random two-liquid excess Gibbs energy model [39]

ODR orthogonal distance regression

PR Peng-Robinson EOS [36]

PR-MC- PR EOS with MC alpha correction and WS

WS-NRTL mixing rule with the NRTL excess Gibbs energy model

SPRT standard platinum resistance thermometer

SW Span-Wagner EOS for CO₂ [6]

TCD thermal conductivity detector in GC

VLE vapor-liquid equilibrium

WS Wong-Sandler mixing rule [38]

Appendix A. Supplementary material

Supplementary material related to this article can be found at <http://dx.doi.org/...>.

References

- [1] S. F. Westman, H. G. J. Stang, S. W. Løvseth, A. Austegard, I. Snustad, S. Ø. Størset, I. S. Ertesvåg, Vapor-liquid equilibrium data for the carbon dioxide and nitrogen (CO₂ + N₂) system at the temperatures 223, 270, 298 and 303 K and pressures up to 18 MPa, *Fluid Phase Equilib.* 409 (2016) 207–241, URL <http://dx.doi.org/10.1016/j.fluid.2015.09.034>.
- [2] S. T. Munkejord, M. Hammer, S. W. Løvseth, CO₂ transport: Data and models – a review, *Appl. Energy* 169 (2016) 499–523, URL <http://dx.doi.org/10.1016/j.apenergy.2016.01.100>.
- [3] J. Gernert, R. Span, EOS-CG: A Helmholtz energy mixture model for humid gases and CCS mixtures, *J. Chem. Thermodyn.* 93 (2016) 274–293, URL <http://dx.doi.org/10.1016/j.jct.2015.05.015>.
- [4] G. J. Gernert, A New Helmholtz Energy Model for Humid Gases and CCS Mixtures, PhD dissertation, Fakultät für Maschinenbau, Ruhr-Universität Bochum, Bochum, URL <http://www-brs.ub.ruhr-uni-bochum.de/netahtml/HSS/Diss/GernertGeorgJohannes/diss.pdf>, 2013.
- [5] H. Li, J. P. Jakobsen, Ø. Wilhelmsen, J. Yan, PVTxy Properties of CO₂ Mixtures Relevant for CO₂ Capture, Transport and Storage: Review of Available Experimental Data and Theoretical Models, *Appl. Energy* 88 (11) (2011) 3567–3579, URL <http://dx.doi.org/10.1016/j.apenergy.2011.03.052>.
- [6] R. Span, W. Wagner, A New Equation of State for Carbon Dioxide Covering the Fluid Region from the Triple-Point Temperature to 1100 K at Pressures up to 800 MPa, *J. Phys. Chem. Ref. Data* 25 (1996) 1509, URL <http://dx.doi.org/10.1063/1.555991>.
- [7] S. W. Løvseth, G. Skaugen, H. G. J. Stang, J. P. Jakobsen, Ø. Wilhelmsen, R. Span, R. Wegge, CO₂Mix Project: Experimental Determination of Thermo-Physical Properties of CO₂-Rich Mixtures, *Energy Procedia* 37 (2013) 2888–2896, URL <http://dx.doi.org/10.1016/j.egypro.2013.06.174>.
- [8] S. W. Løvseth, H. G. J. Stang, A. Austegard, S. F. Westman, R. Span, R. Wegge, Measurements of CO₂-Rich Mixture Properties: Status and CCS Needs, *Energy Procedia* 86 (2016) 469–478, URL <http://dx.doi.org/10.1016/j.egypro.2016.01.048>, the 8th Trondheim Conference on CO₂ Capture, Transport and Storage.
- [9] E. De Visser, C. Hendriks, M. Barrio, M. J. Mølnvik, G. de Koeijer, S. Liljemark, Y. Le Gallo, Dynamis CO₂ Quality Recommendations, *Int. J. Greenhouse Gas Control* 2 (4) (2008) 478–484, URL <http://dx.doi.org/10.1016/j.ijggc.2008.04.006>.
- [10] H. G. J. Stang, S. W. Løvseth, S. Ø. Størset, B. Malvik, H. Rekstad, Accurate Measurements of CO₂ Rich Mixture Phase Equilibria Relevant for CCS Transport and Conditioning, *Energy Procedia* 37 (2013) 2897–2903, URL <http://dx.doi.org/10.1016/j.egypro.2013.06.175>.
- [11] R. D. Chirico, T. W. de Loos, J. Gmehling, A. R. H. Goodwin, S. Gupta, W. M. Haynes, K. N. Marsh, V. Rives, J. D. Olson, C. Spencer, J. F. Brennecke, J. P. M. Trusler, Guidelines for Reporting of Phase Equilibrium Measurements (IUPAC Recommendations 2012), *Pure Appl. Chem.* 84 (8) (2012) 1785–1813, URL <http://dx.doi.org/10.1351/PAC-REC-11-05-02>.
- [12] BIPM, IEC, IFCC, ILAC, IUPAC, IUPAP, ISO, OIML, Evaluation of Measurement Data - Guide for the Expression of Uncertainty in Measurement. JCGM 100: 2008, 2008.
- [13] J. M. S. Fonseca, R. Dohrn, S. Peper, High-pressure fluid-phase equilibria: Experimental methods and systems investigated (2005–2008), *Fluid Phase Equilib.* 300 (1–2) (2011) 1–69, URL <http://dx.doi.org/10.1016/j.fluid.2010.09.017>.
- [14] ARMINES, Patent n° FR 2 853 414, Procédé et dispositif pour prélever des micro-échantillons d'un fluide sous pression contenu dans un contenant, 2003.
- [15] P. Guilbot, A. Valtz, H. Legendre, D. Richon, Rapid on-line sampler-injector: a reliable tool for HT-HP sampling and on-line GC analysis, *Analisis* 28 (5) (2000) 426–431, URL <http://dx.doi.org/10.1051/analisis:2000128>.
- [16] S. F. Westman, H. G. J. Stang, S. Ø. Størset, H. Rekstad, A. Austegard, S. W. Løvseth, Accurate Phase Equilibrium Measurements of CO₂ Mixtures, *Energy Procedia* 51 (2014) 392–401, URL <http://dx.doi.org/10.1016/j.egypro.2014.07.046>.
- [17] M. E. Wieser, T. B. Coplen, Atomic weights of the elements 2009 (IUPAC Technical Report), *Pure Appl. Chem.* 83 (2) (2010) 359–396, URL <http://dx.doi.org/10.1351/PAC-REP-10-09-14>.
- [18] M. E. Wieser, N. Holden, T. B. Coplen, J. K. Böhlke, M. Berglund, W. A. Brand, P. De Bièvre, M. Gröning, R. D. Loss, J. Meija, T. Hirata, T. Prohaska, R. Schoenberg, G. O'Connor, T. Walczyk, S. Yoneda, X.-K. Zhu, Atomic weights of the elements 2011 (IUPAC Technical Report), *Pure Appl. Chem.* 85 (5) (2013) 1047–1078, URL <http://dx.doi.org/10.1351/PAC-REP-13-03-02>.
- [19] G. H. Zenner, L. I. Dana, Liquid-vapor equilibrium compositions of carbon dioxide-oxygen-nitrogen mixtures, in: *Chem. Eng. Prog., Symp. Ser.*, vol. 59, 36–41, 1963.
- [20] A. Fredenslund, G. A. Sather, Gas-liquid equilibrium of the oxygen-carbon dioxide system, *J. Chem. Eng. Data* 15 (1) (1970) 17–22, URL <http://dx.doi.org/10.1021/je60044a024>.
- [21] G. Kaminishi, T. Toriumi, Vapor-Liquid Phase Equilibrium in the CO₂-H₂, CO₂-N₂ and CO₂-O₂ Systems [in Japanese], *Kogyo Kagaku Zasshi* 69 (1966) 175–178, URL http://doi.org/10.1246/nikkashi1898.69.2_175.
- [22] H. S. Booth, J. M. Carter, The Critical Constants of Carbon Dioxide-Oxygen Mixtures, *J. Phys. Chem.* 34 (12) (1930) 2801–2825, URL <http://dx.doi.org/10.1021/j150318a013>.
- [23] N. K. Muirbrook, Experimental and Thermodynamic Study of the High-Pressure Vapor-Liquid Equilibria for the Nitrogen-Oxygen-Carbon Dioxide System, Ph.D. thesis, University of California, Berkeley, 1964.
- [24] W. H. Keesom, Isothermals of mixtures of oxygen and carbon dioxide (with two plates), *Commun. Phys. Lab. Univ. Leiden* 88 (1903) 1–85.
- [25] M. Ahmad, J. Gernert, E. Wilbers, Effect of impurities in captured CO₂ on liquid-vapor equilibrium, *Fluid Phase Equilib.* 363 (2014) 149–155, URL <http://dx.doi.org/10.1016/j.fluid.2013.11.009>.
- [26] A. Fredenslund, J. Møllerup, O. Persson, Gas-liquid equilibrium of oxygen-carbon dioxide system, *J. Chem. Eng. Data* 17 (4) (1972) 440–443, URL <http://dx.doi.org/10.1021/je60055a019>.
- [27] R. Engberg, D. Köpke, R. Eggers, Die Grenzflächenspannungen von CO₂-O₂-und Rauchgas-Mischungen, *Chem. Ing. Tech.* 81 (9) (2009) 1439–1443, URL <http://dx.doi.org/10.1002/cite.200900052>.
- [28] M. S. Green, M. Vicentini-Missoni, J. M. H. Levelt Sengers, Scaling-Law Equation of State for Gases in the Critical Region, *Phys. Rev. Lett.* 18 (1967) 1113–1117, URL <http://dx.doi.org/10.1103/PhysRevLett.18.1113>.
- [29] L. P. Kadanoff, W. Götze, D. Hamblen, R. Hecht, E. A. S. Lewis, V. V. Palciauskas, M. Rayl, J. Swift, D. Aspnas, J. Kane, Static Phenomena Near Critical Points: Theory and Experiment, *Rev. Mod. Phys.* 39 (1967) 395–431, URL <http://dx.doi.org/10.1103/RevModPhys.39.395>.
- [30] M. E. Fisher, The theory of equilibrium critical phenomena, *Rep. Prog. Phys.* 30 (2) (1967) 615, URL <http://dx.doi.org/10.1088/0034-4885/30/2/306>.
- [31] P. Ungerer, B. Tavittian, A. Boutin, Applications of Molecular Simulation in the Oil and Gas Industry. Monte Carlo Methods, chap. 2, Editions Technip, Paris, France, note: Equation 2.100 is lacking the critical composition term, 2005.
- [32] V. Lachet, T. de Bruin, P. Ungerer, C. Coquelet, A. Valtz, V. Hasanov, F. Lockwood, D. Richon, Thermodynamic behavior of the CO₂+SO₂ mixture: Experimental and Monte Carlo simulation studies, *Energy Procedia* 1 (1) (2009) 1641 – 1647, URL <http://dx.doi.org/10.1016/j.egypro.2009.01.215>.
- [33] J. Sengers, J. Levelt Sengers, A universal representation of the thermodynamic properties of fluids in the critical region, *Int. J. Thermophys.* 5 (2) (1984) 195–208, ISSN 0195-928X, URL <http://dx.doi.org/10.1007/BF00505500>.
- [34] H. B. Callen, Thermodynamics and an Introduction to Thermostatistics, Wiley, 2 edn., ISBN 0471862568, 1985.
- [35] O. Kunz, W. Wagner, The GERG-2008 Wide-Range Equation of State for Natural Gases and Other Mixtures: An Expansion of GERG-2004, *J. Chem. Eng. Data* 57 (11) (2012) 3032–3091, URL <http://dx.doi.org/10.1021/je300655b>.
- [36] D.-Y. Peng, D. B. Robinson, A New Two-Constant Equation of State,

- Ind. Eng. Chem. Fundam. 15 (1) (1976) 59–64, URL <http://dx.doi.org/10.1021/i160057a011>.
- [37] P. M. Mathias, T. W. Copeman, Extension of the Peng-Robinson equation of state to complex mixtures: Evaluation of the various forms of the local composition concept, Fluid Phase Equilib. 13 (1983) 91–108, URL [http://dx.doi.org/10.1016/0378-3812\(83\)80084-3](http://dx.doi.org/10.1016/0378-3812(83)80084-3).
- [38] D. S. H. Wong, S. I. Sandler, A Theoretically Correct Mixing Rule for Cubic Equations of State, AIChE J. 38 (5) (1992) 671–680, URL <http://dx.doi.org/10.1002/aic.690380505>.
- [39] H. Renon, J. M. Prausnitz, Local compositions in thermodynamic excess functions for liquid mixtures, AIChE J. 14 (1) (1968) 135–144, URL <http://dx.doi.org/10.1002/aic.690140124>.
- [40] C. Coquelet, A. Valtz, F. Dieu, D. Richon, P. Arpentinier, F. Lockwood, Isothermal P , x , y data for the argon+carbon dioxide system at six temperatures from 233.32 to 299.21 K and pressures up to 14 MPa, Fluid Phase Equilib. 273 (1-2) (2008) 38–43, URL <http://dx.doi.org/10.1016/j.fluid.2008.08.010>.
- [41] P. T. Boggs, R. H. Byrd, J. E. Rogers, R. B. Schnabel, User's Reference Guide for ODRPACK Version 2.01 Software for Weighted Orthogonal Distance Regression, URL http://docs.scipy.org/doc/external/odrpac_guide.pdf, 1992.
- [42] X. Courtial, C.-B. Soo, C. Coquelet, P. Paricaud, D. Ramjugernath, D. Richon, Vapor–liquid equilibrium in the n-butane+methanol system, measurement and modeling from 323.2 to 443.2 K, Fluid Phase Equilib. 277 (2) (2009) 152–161, URL <http://dx.doi.org/10.1016/j.fluid.2008.12.001>.
- [43] O. Chivone-Filho, P. G. Amaral Filho, D. N. Silva, L. R. Terron, Alpha Function for a Series of Hydrocarbons to Peng-Robinson and van der Waals Equations of State, Ind. Eng. Chem. Res. 40 (26) (2001) 6240–6244, URL <http://dx.doi.org/10.1021/ie001134o>.
- [44] R. Schmidt, W. Wagner, A new form of the equation of state for pure substances and its application to oxygen, Fluid Phase Equilib. 19 (3) (1985) 175–200, URL [http://dx.doi.org/10.1016/0378-3812\(85\)87016-3](http://dx.doi.org/10.1016/0378-3812(85)87016-3).
- [45] H. Preston-Thomas, The International Temperature Scale of 1990 (ITS-90), Metrologia 27 (1) (1990) 3–10, URL <http://dx.doi.org/10.1088/0026-1394/27/1/002>.